TORSIONAL STRENGTH OF PRESTRESSED CONCRETE BRIDGE GIRDERS

by

Eugene Buth, Assistant Research Engineer

Howard L. Furr, Research Engineer

Research Report 150-1F

Torsional Strength of Prestressed Concrete Bridge Girders

Research Study Number 2-5-70-150

Sponsored by

The Texas Highway Department
In Cooperation with the
U. S. Department of Transportation, Federal Highway Administration

August 1971

TEXAS TRANSPORTATION INSTITUTE
Texas A&M University
College Station, Texas

DISCLAIMER

The opinions, findings and conclusions expressed in this publication are those of the authors and not necessarily those of the Federal Highway Administration.

ABSTRACT

Two Texas Highway Department type B prestressed concrete bridge girders were tested to determine their torsional strength. Applied torque, angle of twist and strains in the concrete were determined.

The theoretical strength and torque-rotation relationships were calculated by classical elastic theory.

Experimental and theoretical torque-rotation relationships were found to agree very closely. The theoretical torsional strength was on the average about 75 percent of the experimentally determined torsional strength.

SUMMARY

Two Texas Highway Department Type B prestressed concrete bridge girders were loaded to failure in torsion to determine their torsion strength. One girder was made of normal weight concrete and the other of lightweight concrete. The torsional loading was applied to each end of the beam through loading yokes with hydraulic jacks. The angle of twist was measured with a precise level and two scales hanging from cross bars attached to each end of the girder. Strains on the surface of the girder were measured with electrical resistance strain gauge rosettes on cross sections at mid span and 15 ft. either side of mid span.

St. Venant's elastic theory was used to calculate the torsional stiffness and torsional strength of each of the girders.

The effective values of shearing modulus, G, of 2.30 and 1.65×10^6 psi found in the full scale torsion tests, compare well with values of 2.44 and 1.56 psi determined by ASTM C215 for the normal weight and lightweight girders respectively. Theoretically derived torsional capacity using $10\sqrt{f'_c}$ as the ultimate tensile strength was about 75% of the experimental torsional capacity, which is on the conservative side. If splitting tensile strength was used as the ultimate strength, the theoretical torsional capacity was about 50% of the experimental torsional capacity.

IMPLEMENTATION

The test results of the two girders investigated indicate that the present practice of cantilevering forms a maximum distance of 3 feet from the edge girder is sufficiently conservative even if no additional bracing is provided for the girder. On the basis of a maximum unsupported length of 50 ft. the maximum torque created in the forms and deck concrete is in the range of 12 to 16 ft-kips. Ignoring the effect of the presence of flexural stress created by the same load, the torsional load is about 25% of the capacity of the girder indicated by tests in this investigation. This indicated factor of safety of 4 compares well with that of the overall design.

Since this was a limited type B study it was not intended to be a comprehensive and conclusive study. Highway engineers may desire to conduct additional experimental and theoretical work. This study included only the effects of torsional loading, dead load and prestress but no attempt was made to include flexural live loads or restraints offered by diaphragms.

TABLE OF CONTENTS

INTRODUCTION

Present construction practice in casting concrete bridge decks is to cantilever the deck forms from the edge girders on either side of the structure. These deck forms are braced to the bottom of the edge girders which creates a torsional loading on the girders. Existing codes do not specify criteria or methods of analysis for determining the torsional strength of such girders.

The objective of the study was to determine the torsional strength of Texas Highway Department standard type B pretensioned prestressed bridge girders.

Two existing type B girders were available for use in this study. One of these was made of normal weight concrete and the other of lightweight concrete. The girders were tested in an existing loading frame in the Texas Highway Department District 14 Headquarters in Austin, Texas.

NOTATION

T - Externally applied torque, ft-lbs.

T_{cr} - Value of externally applied torque which causes cracking of concrete, ft-lbs.

K - Torsional stiffness constant in Saint Venant's elastic theory, in^4.

ϕ - Stress function in Saint Venant's elastic theory.

δ - Grid spacing, in.

Δ, Δ^2 ... - First, second, ... forward differences of stress function.

G - Shearing modulus of elasticity, psi.

θ - Angle of twist in radians per unit length.

σ - Normal stress, psi.

σ_t - Principal tensile stress, psi.

f_c - Compressive strength of concrete, psi.

f_{sp} - Splitting tensile strength of concrete, psi.

THEORETICAL INVESTIGATION

Saint Venant's elastic theory [1*] for a homogeneous member of uniform cross section subjected to pure torsion was used to determine the theoretical stresses developed in the girder by the applied torque. This technique is the same as that applied by Tamberg [2] in his study of AASHO girders. The theory does not account for any effects caused by the presence of prestressing steel or other reinforcement. The stresses resulting from this analysis are those due to applied torque only but these are combined with stresses due to prestressing and flexural dead load in the calculation of the theoretical strength of the girder. The governing differential equation for the elastic torsional theory is:

$$\frac{\partial^2 \phi}{\partial x^2} + \frac{\partial^2 \phi}{\partial y^2} = -2G\theta \quad \ldots\ldots\ldots\ldots \quad (1)$$

Where: ϕ = stress function

G = shear modulus of elasticity, psi

θ = angle of twist per unit length.

In the application of this theory, the cross section of the girder was divided into a 2 inch square grid. The differential equation written in finite difference form for an interior point is then:

$$\frac{1}{\delta^2} \left(\phi_{i+1} + \phi_{i+2} + \phi_{i+3} + \phi_{i+4} - 4\phi_i\right) = -2G\theta \quad \ldots \quad (2)$$

*Superscript numerals refer to items in the list of references.

For points near the boundary where the grid pattern is not complete, the finite difference equation is modified. The finite difference equation can be written for each point in the grid. This will result in a system of equations which can be solved simultaneously to yield values of ϕ for each point in the grid.

The shear stress attributable to the applied torque only can then be determined by the relationship:

$$\tau_y = \frac{\partial \phi}{\partial x} \quad \text{- - - - - - - - - - - - - - - - - - (3)}$$

This first partial derivative is evaulated using the forward differences method. The equation is:

$$\tau = \frac{1}{\delta^2} \left(\Delta\phi - \frac{1}{2}\Delta^2\phi + \frac{1}{3}\Delta^3\phi - \frac{1}{4}\Delta^4\phi + \ldots\right) \quad \text{- - - - - - (4)}$$

Where Δ, Δ^2 . . . = the first, second, etc. forward difference.

The same values of shear stress can be determined by plotting a cross section of the stress function surface through the point in question and evaluating the slope of this curve at that point. Values of ϕ for the cross section of a type B girder are given in Table 1. Values of the shear stress, in terms of $G\theta$, at various points on the boundary of the cross section are shown in Figure 1. These values of shear stress can be expressed in another very useful form by replacing $G\theta$ with $\frac{T}{K}$.

The relationship between applied torque and angle of twist per unit length is given by:

$$T = KG\theta \quad \text{- - - - - - - - - - - - - - - - - - (5)}$$

Where: T = applied torque in-lbs,

K = torsional stiffness constant, in^4,

G = shear modulus of elasticity, psi, and

θ = angle of twist, radians/in.

Detailed example calculations illustrating the application of this theory are presented in Appendix A.

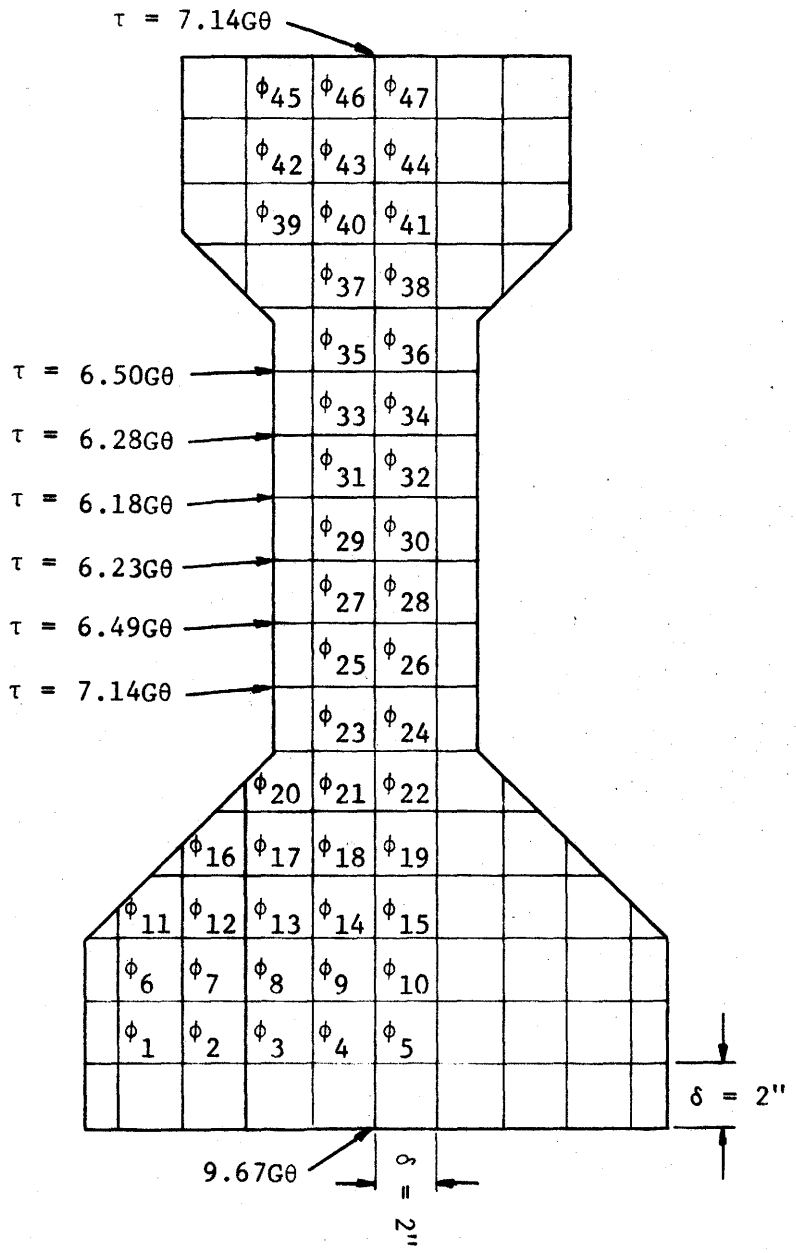

Fig. 1. Cross section of THD type B prestressed girder showing grid system and values of shear stress.

TABLE 1. VALUES FOR ϕ AT THE VARIOUS GRID POINTS IN A THD TYPE B PRESTRESSED CONCRETE GIRDER

Grid Point	Value of ϕ	Grid Point	Value of ϕ	Grid Point	Value of ϕ	Grid Point	Value of ϕ
1*	4.55Gθ	13	20.62Gθ	25	7.77Gθ	37	8.53Gθ
2	9.99	14	25.47	26	12.55	38	13.09
3	13.19	15	27.16	27	7.03	39	6.13
4	14.96	16	5.87	28	11.39	40	13.00
5	15.54	17	16.00	29	6.78	41	15.63
6	5.96	18	22.99	30	10.95	42	8.61
7	14.24	19	25.46	31	6.73	43	13.70
8	19.79	20	6.50	32	10.87	44	15.44
9	23.11	21	17.03	33	6.84	45	6.59
10	24.23	22	20.70	34	11.06	46	9.76
11	4.20	23	9.92	35	7.26	47	10.74
12	13.23	24	15.27	36	11.66		

*See Fig. 1 for grid point locations. Values of ϕ are symmetric about the vertical centerline of the cross-section.

EXPERIMENTAL INVESTIGATION

Two standard THD type B pretensioned, prestress, draped strand girders 50 feet long were available for testing. Cross-sectional dimensions of these girders are shown in Figure 2. One girder was of lightweight and the other normal weight concrete. The concrete of the lightweight girder was made from lightweight coarse aggregate and natural sand. For more details concerning these girders, the reader is referred to reference 4 wherein they are denoted LW and NW (cast 3/20/68).

An existing testing frame which was designed and constructed by THD for structural testing of prestressed bridge girders was used to apply the load to the beams. This facility with a failed girder installed is illustrated in Figure 3. Load was applied to both ends of the girder with hydraulic jacks and bourdon gauges were used to determine the amount of load.

Rotational displacements of each end of the girder were determined by use of a precise level and two scales hanging from cross-bars attached to each end of the girder. This setup is illustrated in Figure 4.

Electrical resistance rectangular strain gauge rosettes were installed on the surface of each girder at the locations shown in Figure 2. The gauges had 120 ohms resistance and 2.362 in. gauge length. These gauges were installed while the girder was simply supported in the testing frame with no external load applied. The strains due to dead load and prestress already existed when the

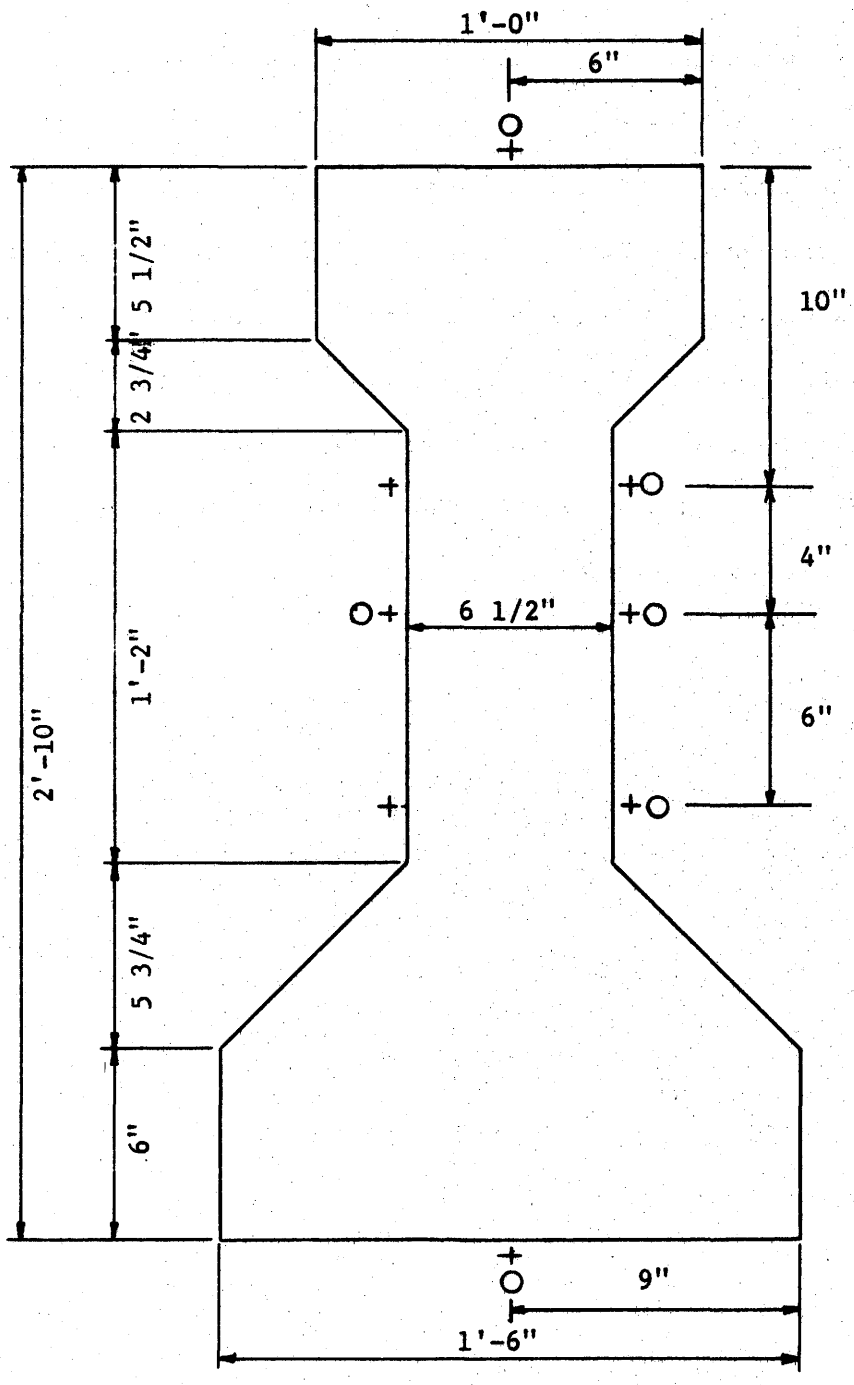

+ gauges at mid span

O gauges at 15' either side of mid span

Fig. 2. Cross-section of THD type B girder showing dimensions and locations of strain gauge rosettes.

gauges were installed and the strains measured by these gauges were those due to the applied torque only. The orientation of the gauges was such that the three arms made angles of zero, 45 and 90 degrees with the longitudinal axis of the girder. Switching and balancing units and digital readout equipment were used to read these gauges.

Load increments of 735 lbs. (1000 psi on the bourdon gauges) were applied to the girder. After each load increment, the rotational displacement of each end of the girder and the strain at each gauge location were determined.

Fig. 3. Testing frame with failed specimen.

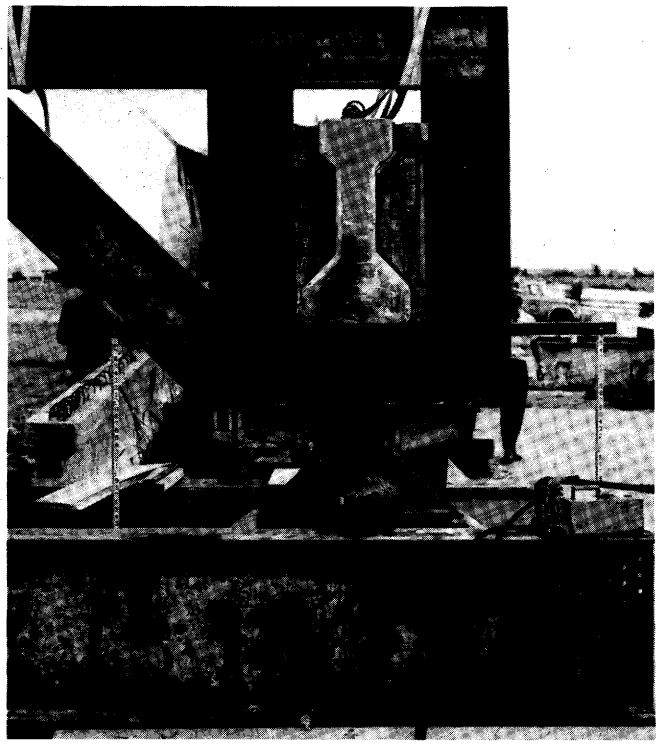

Fig. 4. End view of testing frame showing scales used to determine rotational displacements of end of specimen.

DISCUSSION OF RESULTS

Normal Weight Girder Test

The first sign of distress in this girder was noted at the support on the south end when, at a torque of 35.2 ft-kips, a small piece of concrete was sheared out of the girder. A diagonal crack then appeared in the web extending to the top flange adjacent to this support. Examination of this specimen showed that this was a local condition caused by high pressure of the twisting frame against the beam and not a condition caused by or influencing the torsional strength of the girder. Once this cracking occurred and allowed for redistribution of stress at the point of loading it did not progress further.

At a torque of 41.2 ft-kips a 2 inch long diagonal crack was observed at about mid depth of the web 15 feet from the north end of the girder on the east side. The crack did not grow with added torque and it is believed that the crack was caused by a small local imperfection. It did not appear to influence the strength of the girder. The first diagonal crack caused by the torsional load was observed when the applied torque was 88.8 ft-kips. This crack extended from the bottom flange diagonally through the web and upper flange on the west side of the girder near the south end.

The crack which resulted in failure occurred at an applied torque of 91.2 ft-kips and passed through the hold down point of the prestressing steel on the north end of the girder. The crack was initially

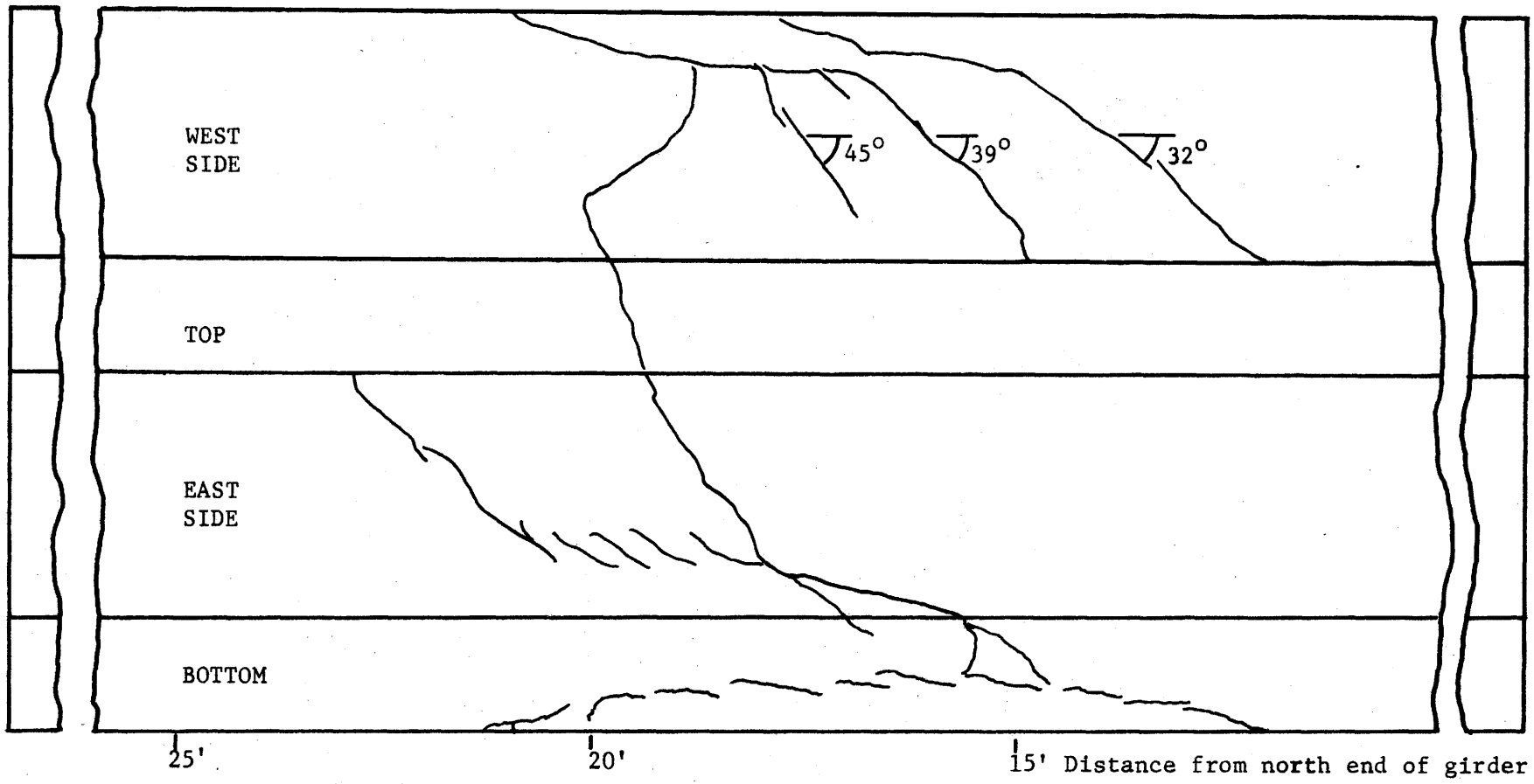

Fig. 5. Cracking pattern in normal weight girder.

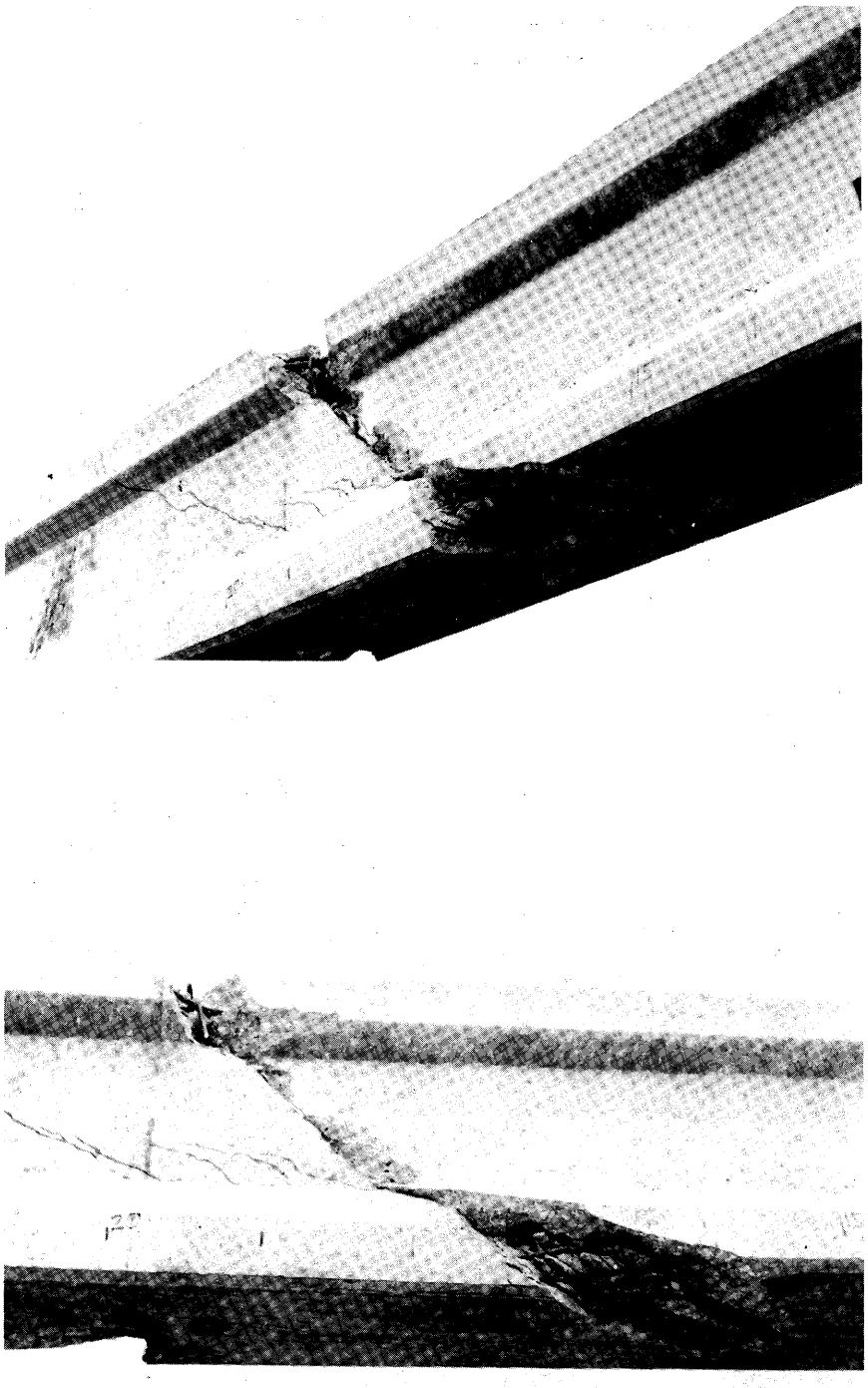

Fig. 6. Photo of failure in normal weight girder.

observed to extend from a point where the bottom flange joins the web diagonally to the top of the girder. The crack projected across the top flange and diagonally down the other side of the girder forming a helical shape. The two ends of the helix were connected by a longitudinal crack in the bottom flange. The crack pattern developed in this girder is illustrated in Figure 5 and the failure crack is illustrated in Figure 6.

Lightweight Girder Test

The same type of local cracking occurred at the loading frame on the south end as it did with the normal weight girder. This distress occurred at torques below 41.2 ft-kips. At a torque of 41.2 ft-kips a diagonal crack occurred adjacent to the support at the south end but neither of these cracks grew any further as loading continued. At 82.3 ft-kips of torque diagonal cracking began to occur in the top flange and web. These cracks developed at several locations along the length of the girder while the torque was being held at 82.3 ft-kips. The girder failed while the strain gauges were being read at this level of torque. The crack pattern developed in this girder is illustrated in Figure 7 and the failure crack is illustrated in Figure 8.

Experimental Strains

The strains measured by the arms of the strain gauge rosettes which were at 45° angles to the longitudinal axis of the girder were the principal strains due to the applied torque. This fact was verified

experimentally by the nil strains measured in the longitudinal and transverse directions. The magnitude of these strains at levels of torque of 76.8, 82.4, 88.8 and 91.2 ft-kips for the normal weight girder are given in Figure 9 and at levels of torque at 64.8, 70.4, 76.8 and 82.4 ft-kips for the lightweight girder in Figure 11.

Experimental Stresses

Values of shearing stress were calculated from the measured strains. The strains due to dead load and prestress already existed when the strain gages were installed; therefore, the strains measured were due to applied torque only. They relate to stress in the following manner:

Consider a point on the surface of the cross section of the girder subjected to a torsional loading as illustrated.

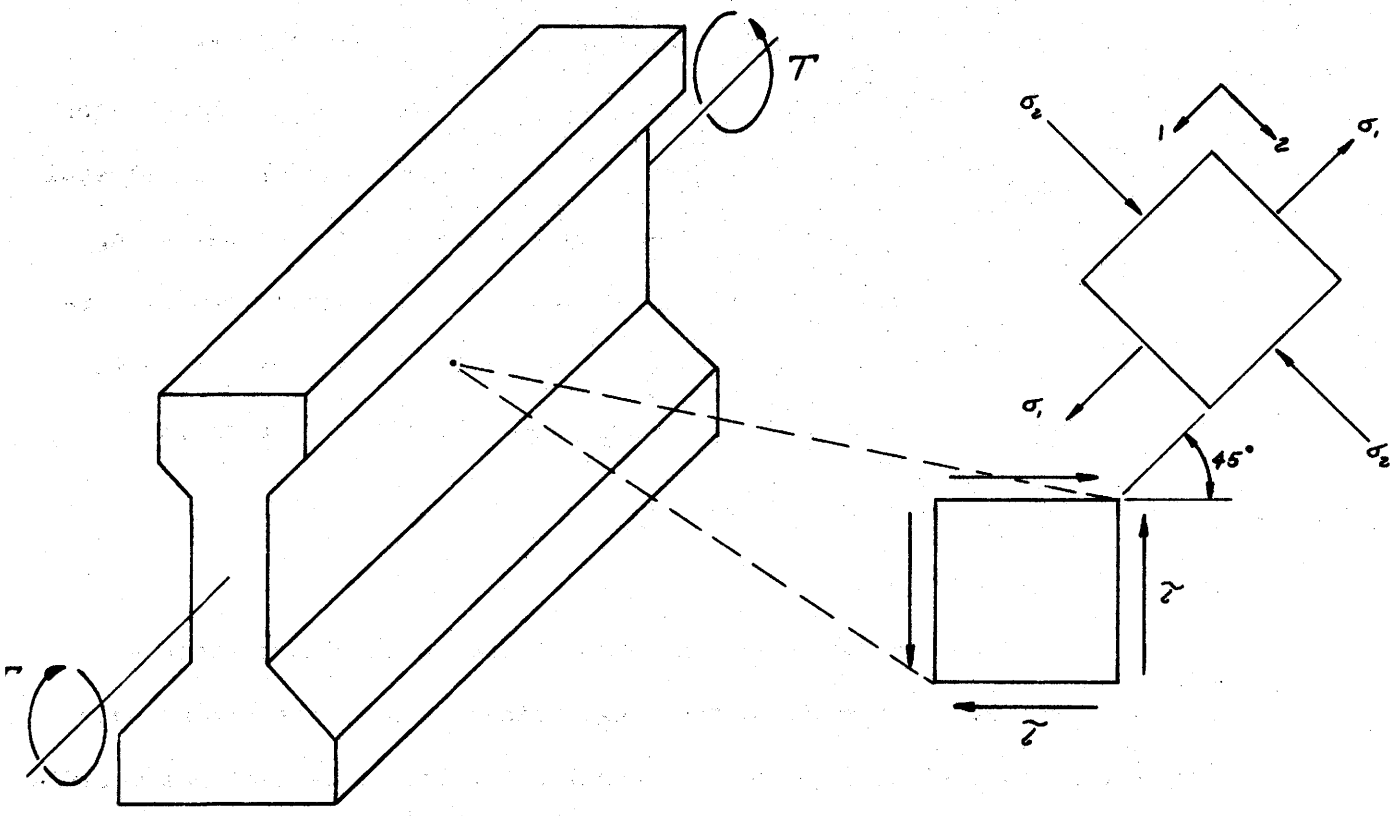

For a point subjected to pure shear the following three equations are valid.

$$\sigma_1 = -\sigma_2 = \tau$$

$$\varepsilon_1 = (\sigma_1 - \mu\sigma_2)/E$$

$$\varepsilon_2 = (\sigma_2 - \mu\sigma_1)/E$$

These equations and $G = \frac{E}{2(1+\mu)}$ will yield:

$$\tau = 2G\varepsilon \quad (6)$$

The shear stress was calculated, using equation 6, for each point where the strain was experimentally measured. These values of shear stress, which are equal in magnitude to the principal tensile stress at that point, are presented in Figures 10 and 12.

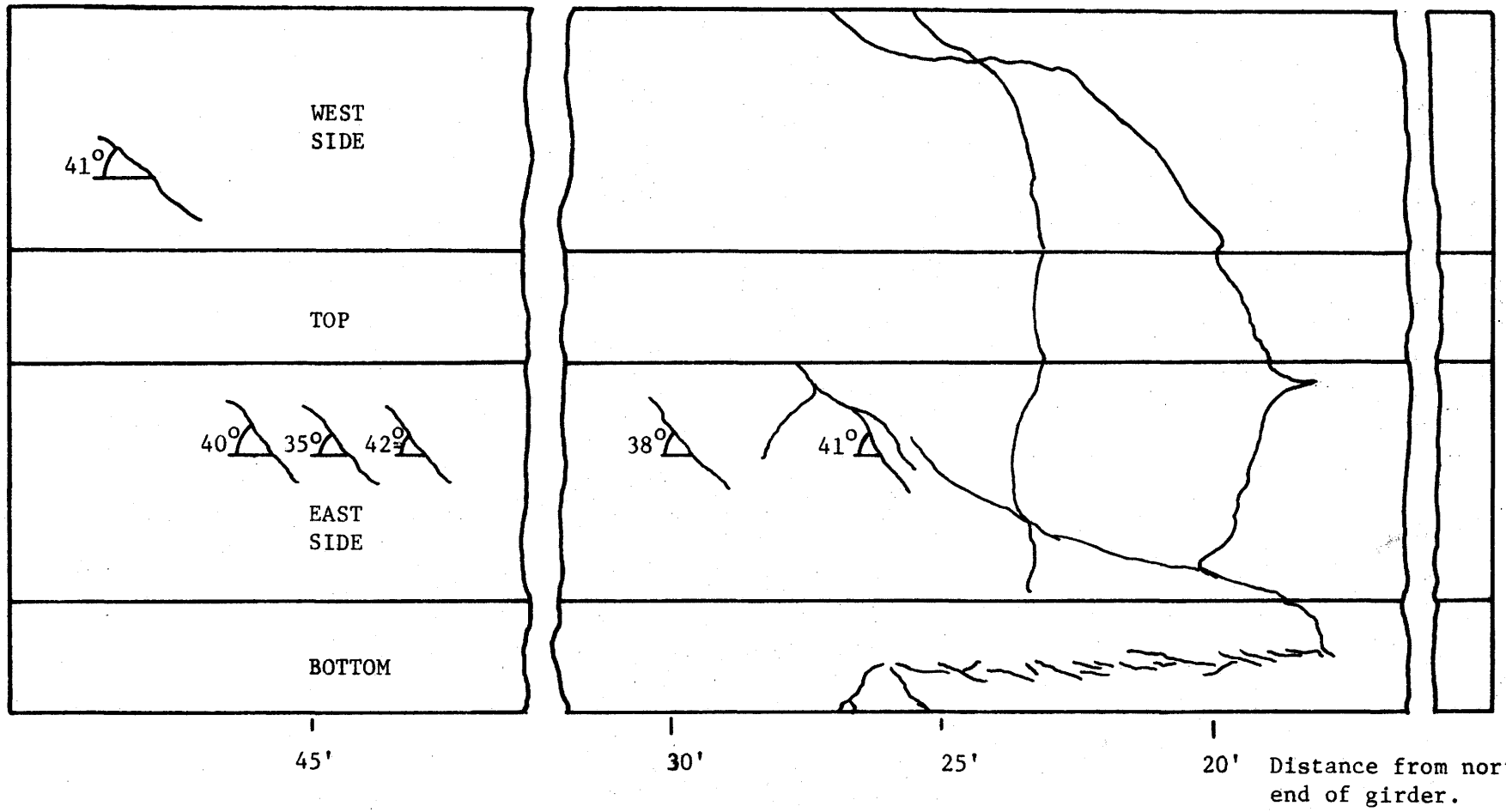

Figure 7. Cracking pattern in lightweight girder.

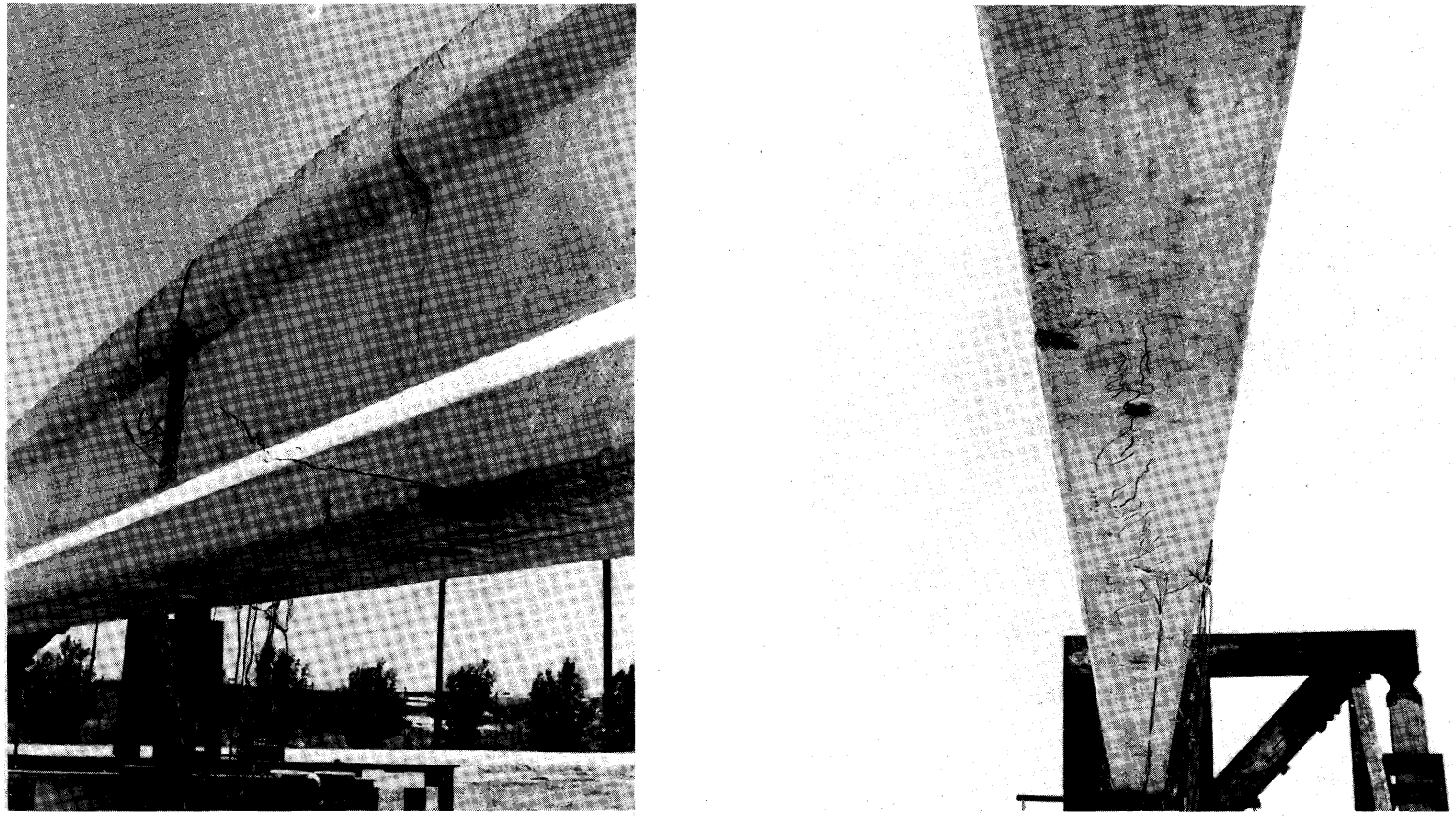

Fig. 8. Photo of failure crack in lightweight girder.

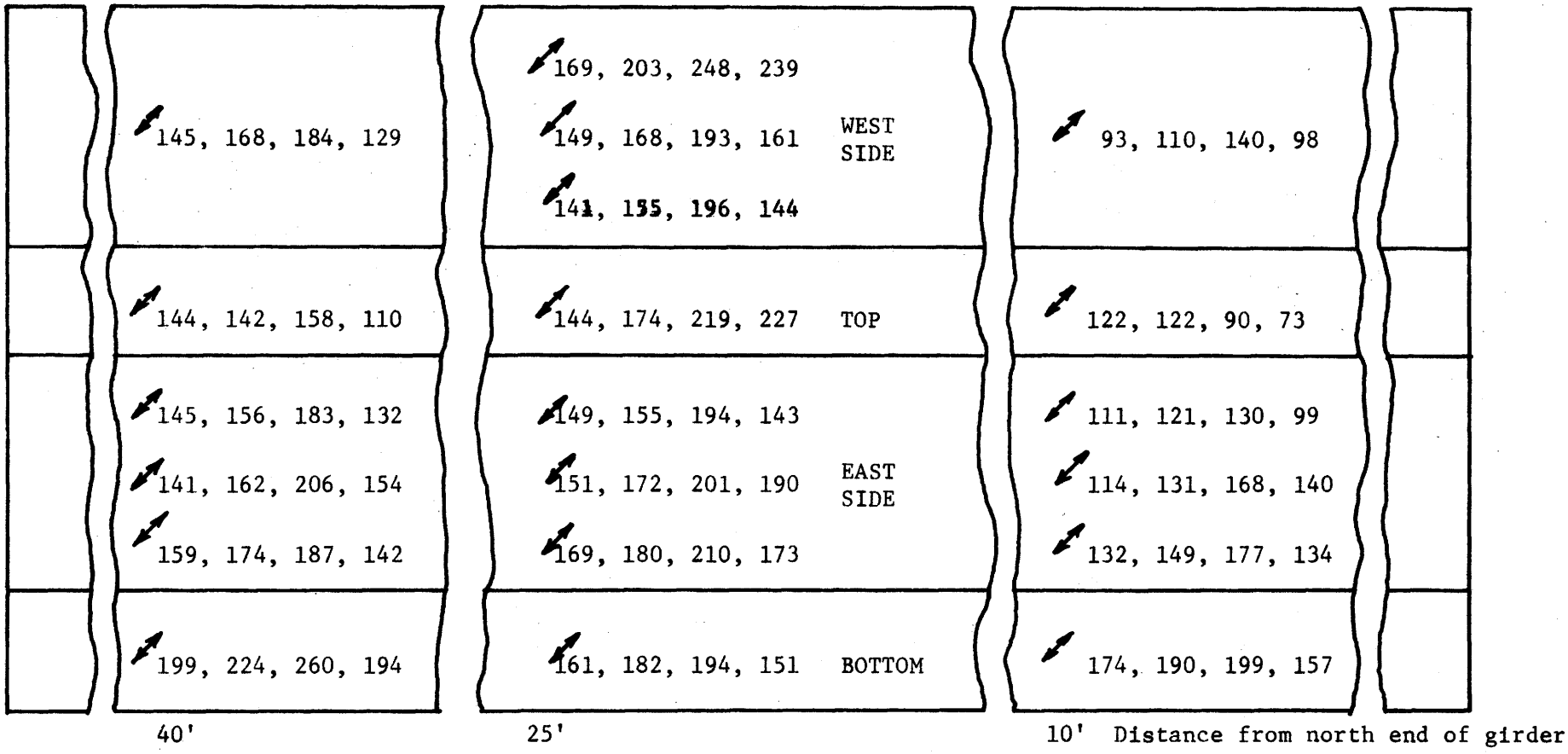

Fig. 9. Strains in micro-in. per in. (due to applied torque only) at torques of 76.8, 82.4, 88.8 and 91.2 ft-kips for normal weight girder.

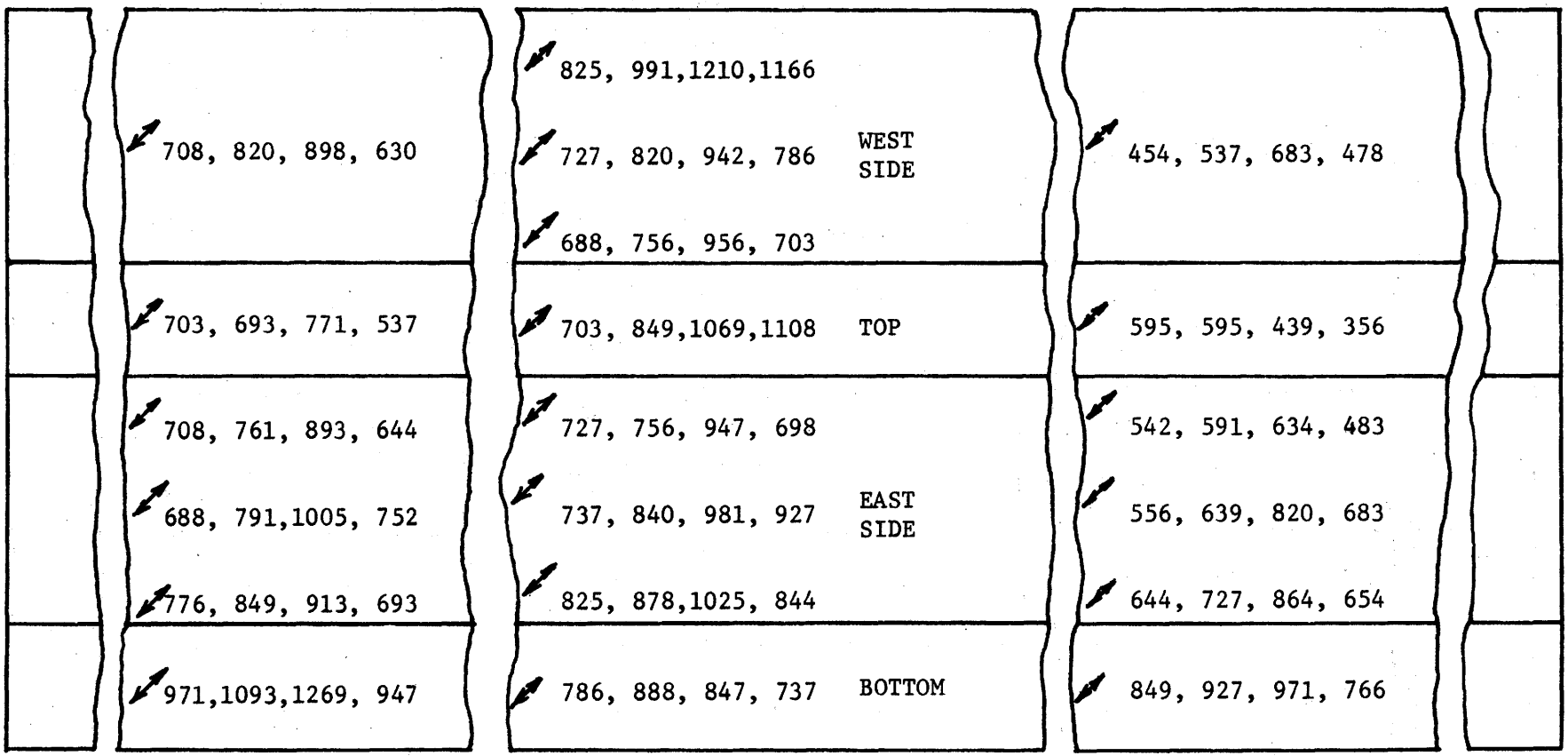

Figure 10: Stresses computed from measured strains.

Change in stresses, due to applied torque only, at torques of 76.8, 82.4, 88.8, and 91.2 ft-kips for normal weight girder. Note that stresses due to dead load and prestress are not reflected in these numbers.

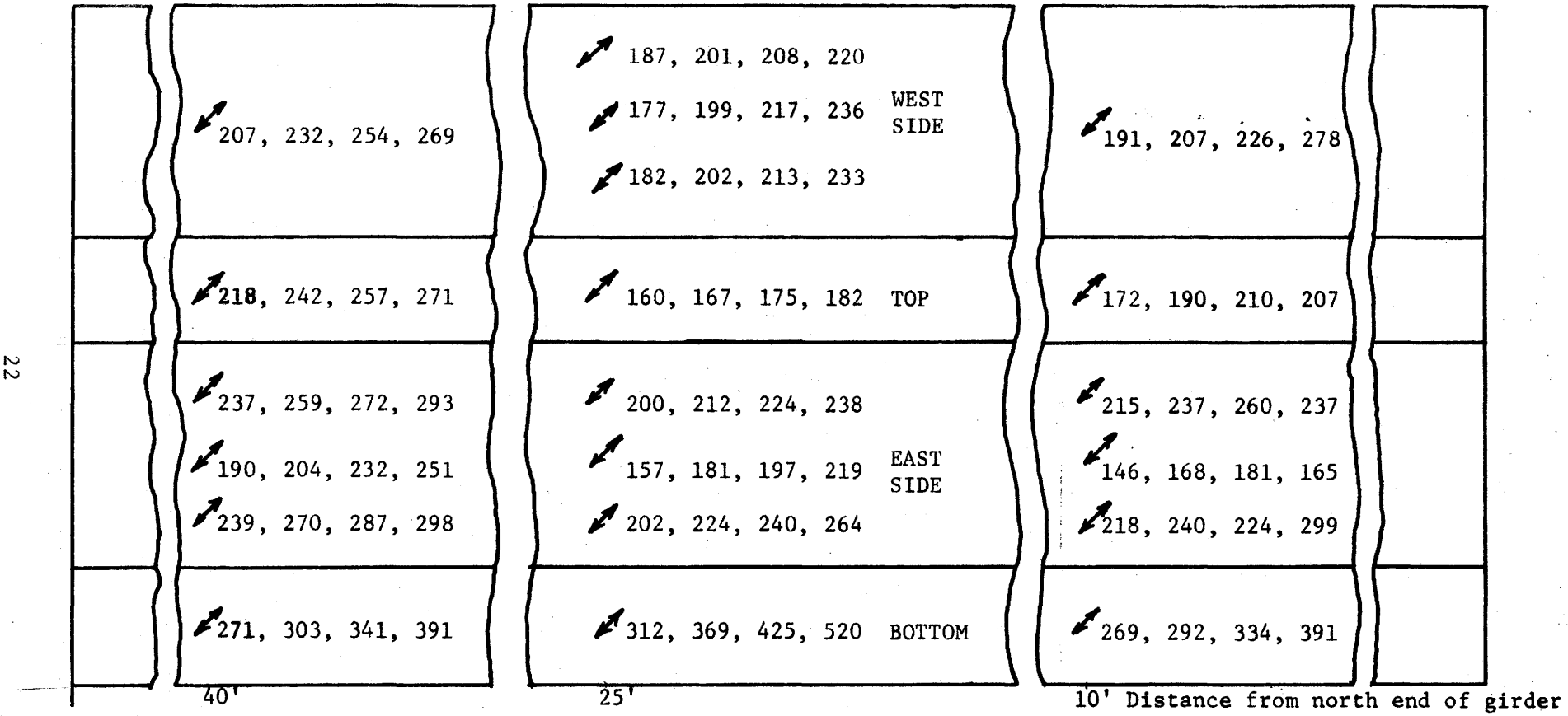

Fig. 11. Strains in micro-in. per in. (due to applied torque only) at torques of 64.8, 70.4 76.8 and 82.4 ft-kips for lightweight concrete girder.

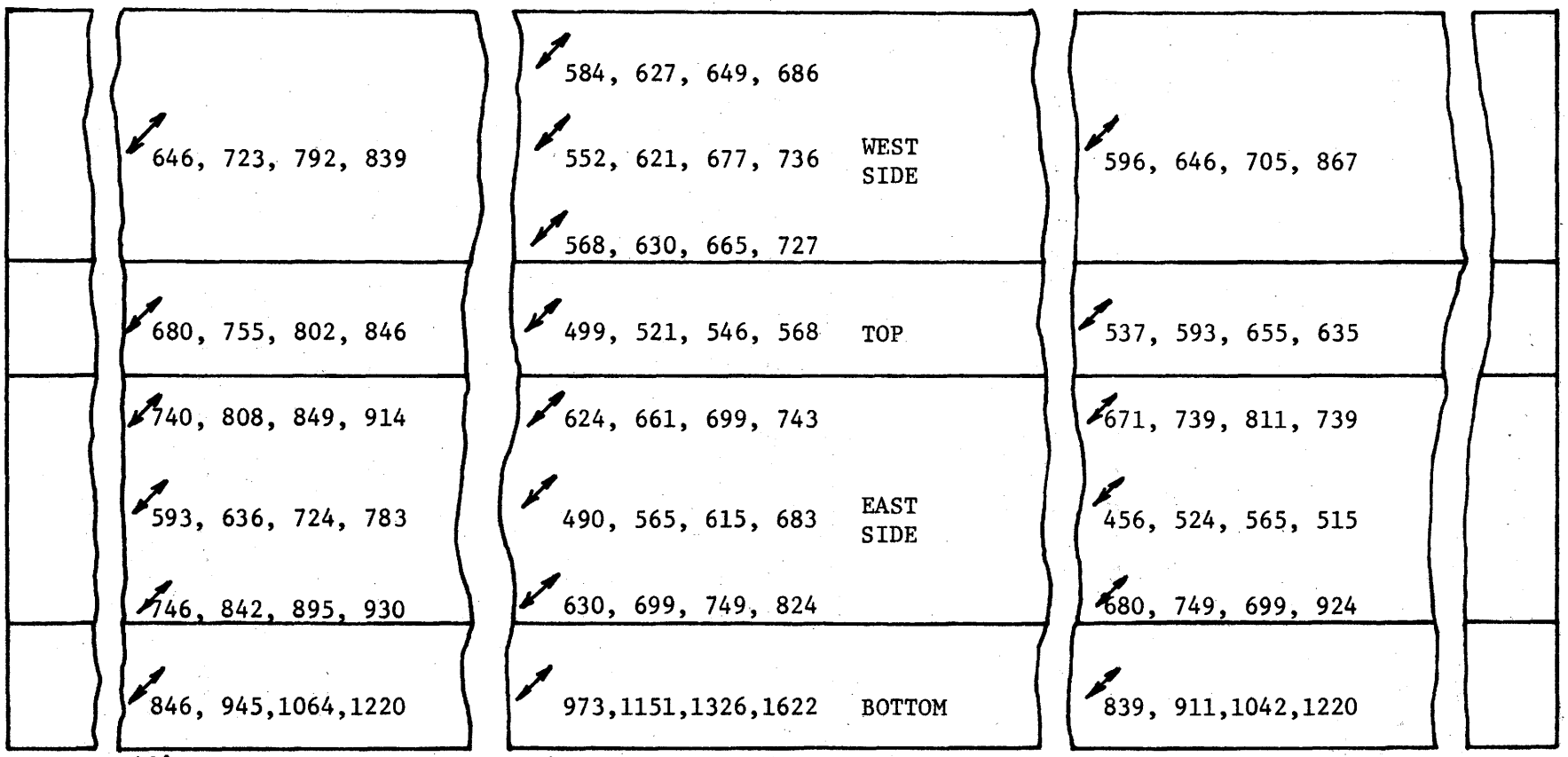

Figure 12: Stresses computed from measured strains

Change in stresses, due to applied toruqe only, at torques of 64.8, 70.4, 76.8 and 82.4 ft-kips for lightweight girder. Note that stresses due to dead load and prestress are not reflected in these numbers.

Comparison of theoretical with experimental results

The relationships between the torque and angle of twist for the two girders are illustrated in Figures 13 and 14. On each graph a line has been drawn through the portion of the curve most nearly approximating a straight line. This line is assumed to be the slope of the torque-rotation relationship. Using these data with K = 7,600 in^4 the expression $T = KG\Theta$ or $\frac{1}{K}\frac{T}{\Theta} = G$, one finds G to be 2.30 and $1.65X10^6$ psi for the normal weight and lightweight girders respectively. This compares with values of G = 2.44 and $1.56X10^6$ psi determined by ASTM C215, "Test for Fundamental Transverse, Longitudinal, and Torsional Frequencies of Concrete Specimens", for the two girders.

If the stresses due to the applied torque are combined with those due to prestress and dead load the resulting principal stresses (neglecting stress concentrations at the reentrant corners) are greatest in the middle of the face of the top flange at points 5 ft. on either side of midspan of the girder. The expressions relating maximum tensile stress to applied torque are:

$$\sigma_t = 68.5 + \sqrt{4700 + 127.3\ T_{cr}^2} \quad - - - - - - - - - - - \quad (8)$$

and

$$\sigma_t = 116.6 + \sqrt{13,6000 + 127.3\ T_{cr}^2} \quad - - - - - - - - - - - \quad (9)$$

for the normal weight and lightweight girders respectively. A more detailed treatment of these relationships is given in Appendix C. If the tensile strength of the concrete is taken as 10 f'_c, the resulting torques necessary to cause cracking of the concrete as 66.1 ft-kips for the normal weight and 66.5 ft-kips for the lightweight girder.

Two standard 6X12 cylinders were available for each of the girders.

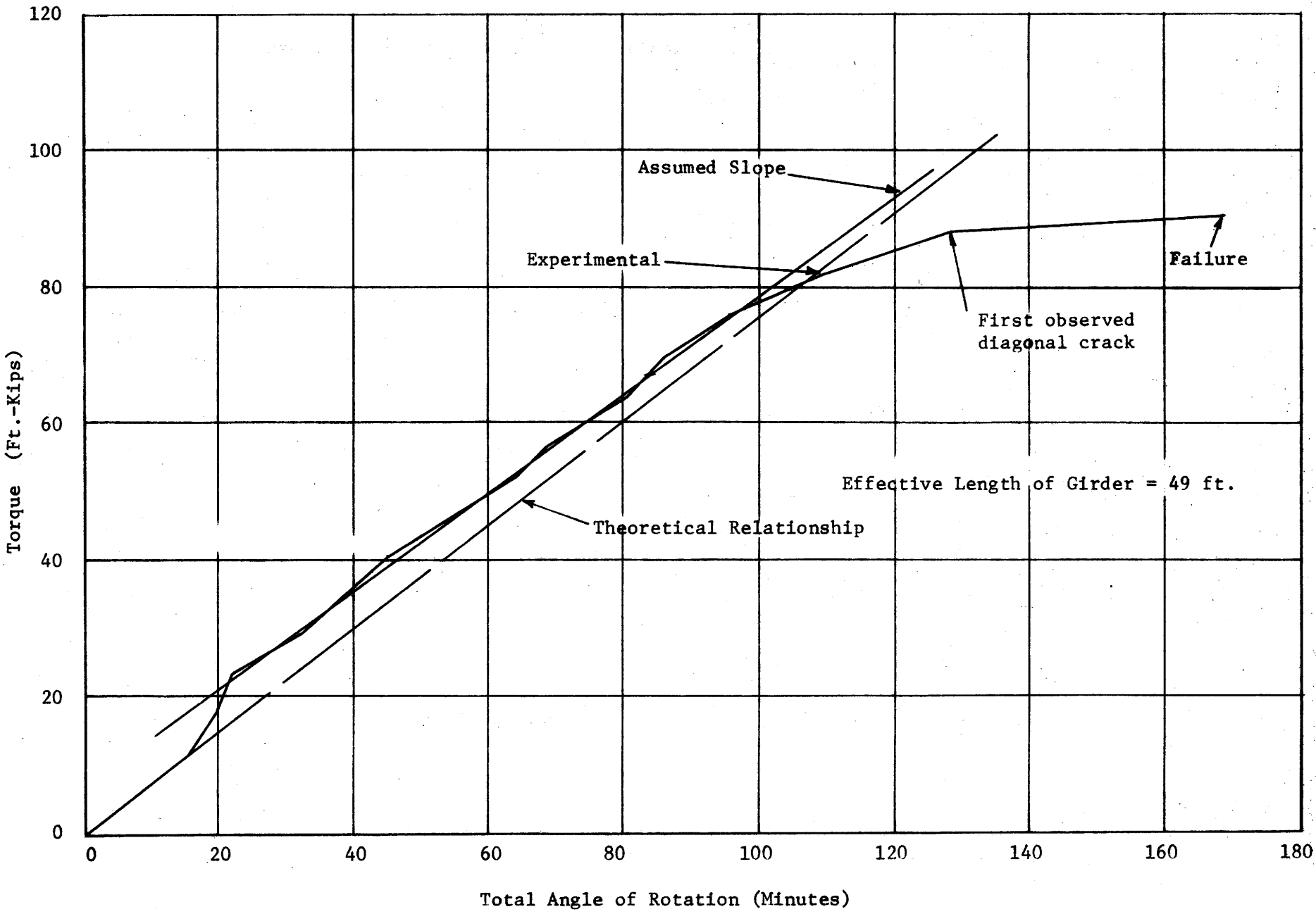

Fig. 13. Torque-rotation relationship for normal weight girder.

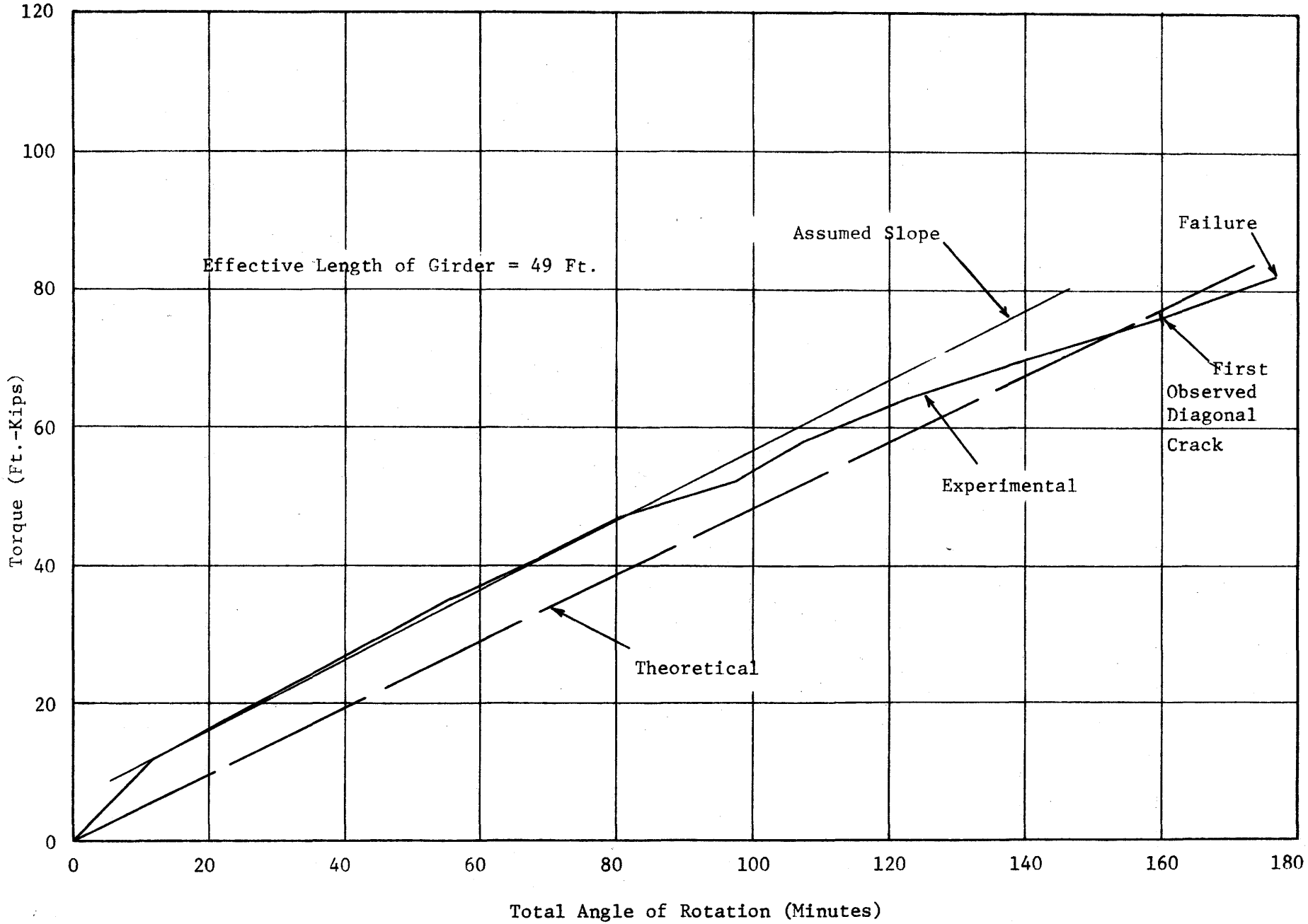

Fig. 14. Torque-rotation relationship for lightweight concrete girder.

Splitting tensile tests were conducted on these cylinders in the Texas Transportation Institute laboratory. The splitting tensile strength was 540 psi for the lightweight concrete and 560 psi for the normal weight concrete. If these values are used in the above expressions, the torques necessary to cause cracking are 36.1 ft-kips for the lightweight and 44.1 ft-kips for the normal weight girders. For the normal weight girder the first observed diagonal crack, other than the 2 in. long diagonal crack observed at 41.2 ft-kips and whose origin is not known, occurred at a torque of 88.5 ft-kips. However, the shape of the torque rotation curve indicates that some unobserved cracking may have occurred at a torque as low as 76.5 ft-kips. The torque-rotation curve for the lightweight girder indicates that unobserved cracking may have occurred at 65.0 ft-kips and some as low as 47.0 ft-kips. Computations were made for selected points on the two girders at selected values of applied torque for comparisons between theoretical and experimental shear stresses. The experimental values were calculated using equation 6 and the theoretical values were determined using the relationships given in Figure 1, with $G\Theta$ replaced by T/K. These values are presented and compared in Table 3 and 4.

TABLE 3

THEORETICAL AND EXPERIMENTAL TORSIONAL STRESSES

FOR LIGHTWEIGHT GIRDER

Applied Torque ft-kips	Point**	$\tau_{exp} = 2G\varepsilon$*	$\tau_{theory} = \frac{CT}{K}$	$\frac{\tau_{theory}}{\tau_{exp}}$
64.8	A40	680	730	1.17
	E40	846	988	1.17
70.4	A40	755	793	1.05
	E40	945	1070	1.13
76.8	A40	802	865	1.08
	E40	1064	1170	1.10
82.4	A40	846	928	1.10
	E40	1220	1253	1.03
64.8	A25	499	730	1.46
	E25	973	988	1.02
70.4	A25	521	793	1.52
	E25	1151	1070	0.93
76.8	A25	546	865	1.58
	E25	1326	1170	0.88
82.4	A25	568	928	1.63
	E25	1622	1253	0.77
64.8	A10	537	730	1.36
	E10	839	988	1.18
70.4	A10	593	793	1.34
	E10	911	1070	1.17
76.8	A10	655	865	1.32
	E10	1042	1170	1.12
82.4	A10	635	928	1.46
	E10	1220	1253	1.03

*$G = 1.56 \times 10^6$

** Points A are on center line of face of top flange, points E are on the center line of bottom flange. Numerical suffix indicates distance from end of girder.

TABLE 4

THEORETICAL AND EXPERIMENTAL TORSIONAL STRESSES

FOR NORMAL WEIGHT GIRDER

Applied Torque ft-kips	Point	$\tau_{exp} = 2G\varepsilon$*	$\tau_{theory} = \frac{CT}{K}$	$\frac{\tau_{theory}}{\tau_{exp}}$
76.8	A40	703	866	1.23
	E40	971	1172	1.21
82.4	A40	693	928	1.34
	E40	1093	1258	1.15
88.8	A40	771	1001	1.30
	E40	1269	1355	1.07
91.2	A40	537	1028	1.91
	E40	948	1392	1.47
76.8	A25	703	866	1.23
	E25	786	1172	1.49
82.4	A25	849	928	1.09
	E25	888	1258	1.42
88.8	A25	1069	1001	.94
	E25	947	1355	1.43
91.2	A25	1108	1028	.93
	E25	737	1392	1.89
76.8	A10	595	866	1.46
	E10	849	1172	1.38
82.4	A10	595	928	1.60
	E10	927	1258	1.36
88.8	A10	439	1001	2.28
	E10	971	1355	1.40
91.2	A10	356	1028	2.89
	E10	766	1392	1.82

*$G = 2.44 \times 10^6$

Stress concentrations

The torsional shear stress is increased in magnitude at reentrant corners of a cross section. The amount of stress concentration is dependent upon the angle of the corner and the radius that exists between the two adjoining faces. Calculations were made to determine the shear stress at the reentrant corners between the top flange and the web and between the bottom flange and the web of the girders. The values of these shear stresses are 11.80 GΘ and 10.9 GΘ for the reentrant corners at the top and bottom flanges respectively. For the top flange reentrant corners at points five feet either side of midspan of the girder, the expressions for principal tensile stress are:

$$\sigma_t = -134 + \sqrt{17{,}950 + (11.80G\Theta)^2} \quad - - - - - - - - - \quad -(10)$$

$$\sigma_t = -165 + \sqrt{27{,}200 + (11.80G\Theta)^2} \quad - - - - - - - - - \quad -(11)$$

for the lightweight and normal weight girders respectively. Equations 8 and 10 are compared in Figure 15a and equations 9 and 11 are compared in Figure 15b. From these plots, it is seen that the location of the point on the girder where the maximum tensile stress occurs is dependent upon the relative magnitude of the applied torque and the bending stresses. The stresses at the reentrant corner do not exceed those in the top flange for low value torques. For values of torque near the failure torque, the concentrated stresses at the reentrant corner significantly exceed those in the top flange. It should be remembered that the stress concentrations are confined to a very small area and that

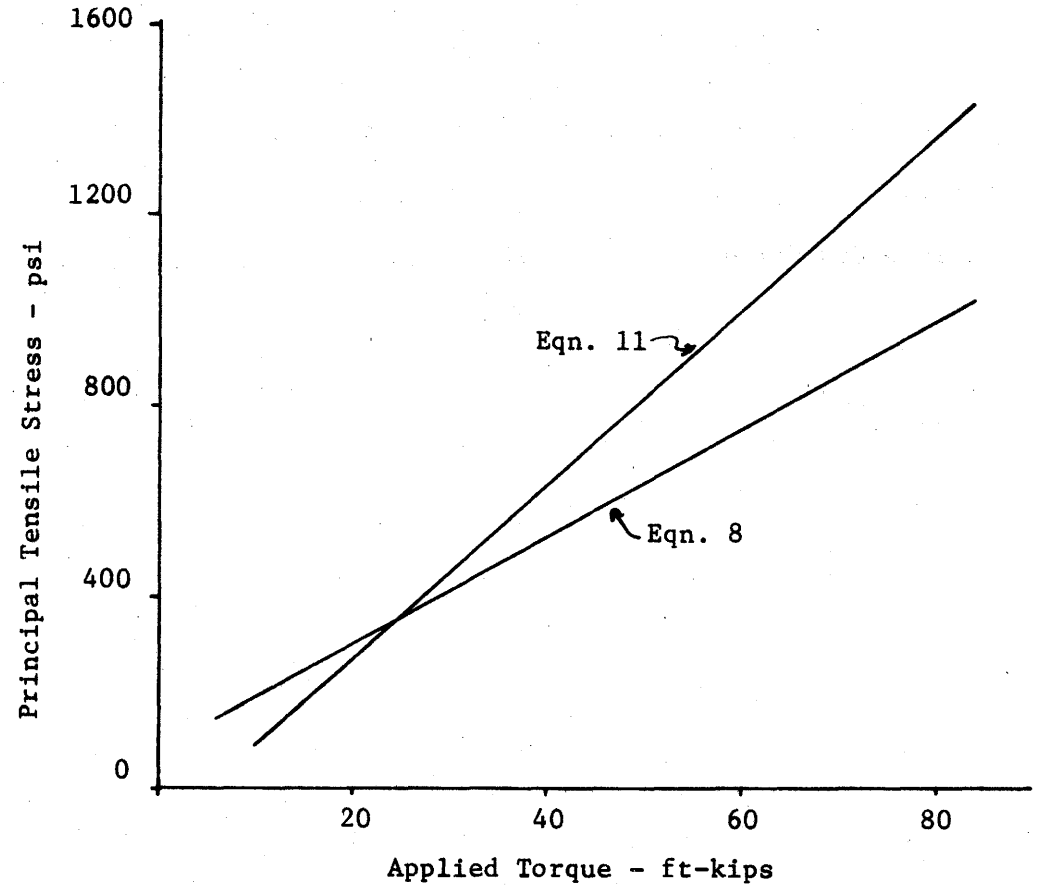

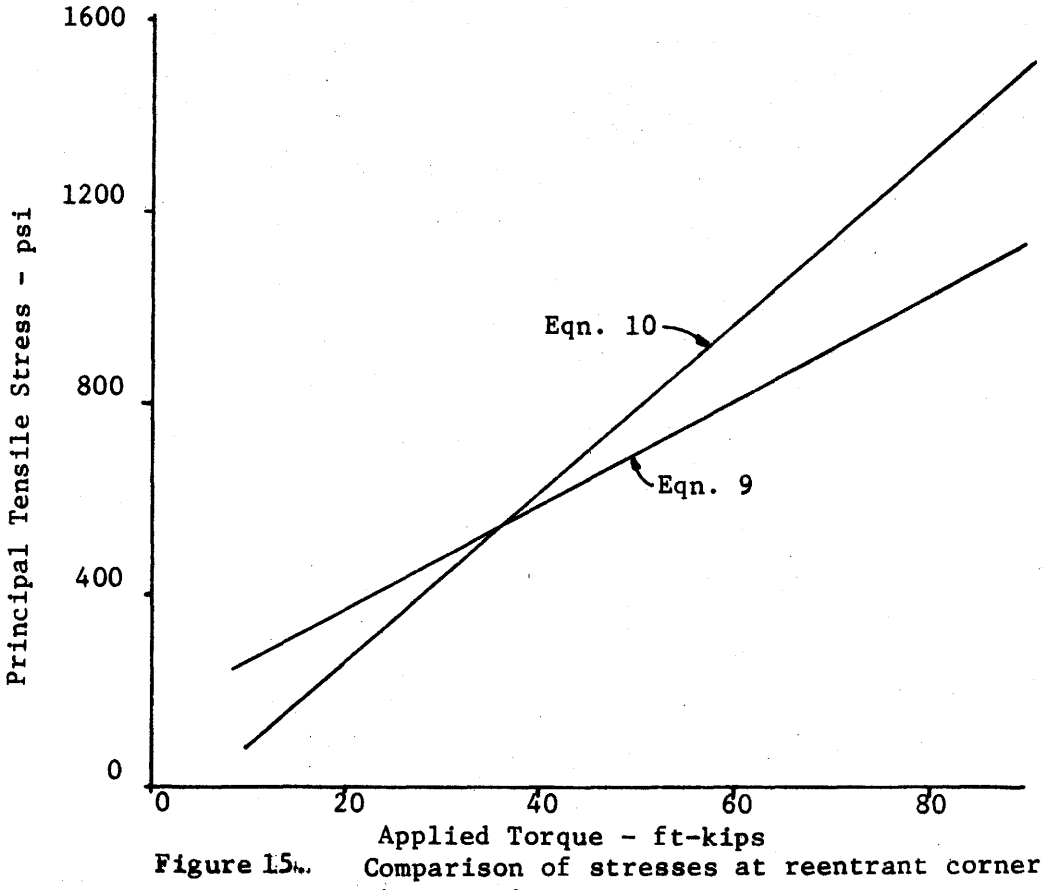

Figure 15. Comparison of stresses at reentrant corner with stresses in top flange.

significantly lower stresses exist either side of the corner. Localized plastic yielding could account for the fact that pronounced early failure did not occur at the reentrant corner in the tests.

CONCLUSION

On the basis of the two tests and the analysis conducted in this study the following conclusions are indicated.

(1) When subjected to a torsional load, the prestressed concrete girders failed in tension along a diagonal line which made an angle of approximately 40 degrees on the sides and 50 degrees on the top flange. The ends of this crack were connected by a line on the bottom flange running longitudinally with the axis of the girder.

(2) The effective values of shearing modulus, G, of 2.30 and 1.65X 10^6 psi found in the full scale torsion tests compare well with values of 2.44 and 1.56X10^6 psi determined by ASTM C215 for the normal weight and lightweight girders respectively.

(3) Theoretically derived torsional capacity using $10\sqrt{f'_c}$ as the ultimate tensile strength was about 75 percent of the experimental torsional capacity, which is on the conservative side. If strengths obtained from split cylinder tests are used as the ultimate strength the theoretical torsional capacity is about 50 percent of the experimental torsional capacity.

REFERENCES

1. Timoshenko, S. and Goodier, J. N., Theory of Elasticity, Second Edition, McGraw-Hill, New York, 1951.

2. Tamberg, K. G., "Elastic Torsional Stiffness of Prestressed Concrete AASHO Girders," Journal of American Concrete Institute, Proceedings, V. 62, No. 4, April 1965.

3. Gersch, B. C. and Moore, Willard H., "Flexure, Shear and Torsion Tests on Prestressed Concrete I-Beam," Highway Research Board Bulletin 339, Washington, D. C., 1962.

4. Furr, H. L., Sinno, R., and Ingram, L. I., "Prestress Loss and Creep Camber in Highway Bridge with Reinforced Concrete Slab on Pretensioned Prestressed Concrete Beams," Research Report No. 69-3 (Final) Texas Transportation Institute, Texas A&M University, Oct. 1968.

5. Zia, Paul, "Torsional Strength of Prestressed Concrete Members," Journal of the American Concrete Institute, Proceedings, V. 57, April 1961.

6. Gesund, Hans, and Boston, L. A., "Ultimate Strength in Combined Bending and Torsion of Concrete Beams Containing Only Logitudinal Reinforcement," Journal of the American Concrete Institute, Proceedings, V. 61, November 1964.

7. Walsh, et.al, "The Ultimate Strength Design of Rectangular Reinforced Concrete Beams Subjected to Combined Torsion, Bending and Shear," Civil Engineering Transactions, The Institute of Engineers, Australia, October 1966.

8. Hsu, T. T. C., "Torsion of Structural Concrete-Uniformly Prestressed Rectangular Members without Web Reinforcement," Journal of Prestressed Concrete Institute, April 1968.

9. Higdon, A., Ohlsen, E. H., Stiles, W. B., and Weese, J. A., Mechanics of Materials, Second Edition, John Wiley and Sons, Inc., New York, 1968.

APPENDIX A

APPENDIX A

Method for calculating shear stresses and torsional stiffness, "K".[1,2]

Outline of Steps:

(a) Layout a square grid on the cross section and number each point.

(b) For each point of the grid, write the finite difference form of the equation $\frac{\partial^2\phi}{\partial x^2} + \frac{\partial^2\phi}{\partial y^2} = -2G\theta$.

This will result in a system of equations which can be solved simultaneously for values of ϕ in terms of $G\theta$. This can best be done using a matrix inversion and multiplication routine on the computer. Such a routine was used in this study.

(c) Using numerical techniques, evaluate the intergal

$$T = 2 \int_{area} \phi dxdy = KG\theta$$

(d) Solve this expression for the torsional stiffness "K". Note that the integral will be in terms of $G\theta$ and that $G\theta$ will cancel out of this expression. K is a property of the geometry of the cross section only and does not reflect any properties of the material such as shear modulus, strength, presence of prestress, etc.

This procedure is the shortest and simplist known and calculations were not made for beams other than THD types B&C. However, once the value of K is calculated for any given cross section, the value will not change for

that cross section. Values of K for AASHO girders given by Tamberg are: Type I - 4,900 in.^{4}, Type II - 8,300 in.^{4}, Type III - 19,000 in.^{4} and Type IV - 34,500 in.^{4}.

The following set of calculations were made for a THD type C beam and will illustrate the application of the procedure outlined above. The governing differential equation is evaluated numerically as follows:

$$\frac{\partial^2\phi}{\partial x^2} + \frac{\partial^2\phi}{\partial y^2} = -2G\theta \qquad \text{(1)}$$

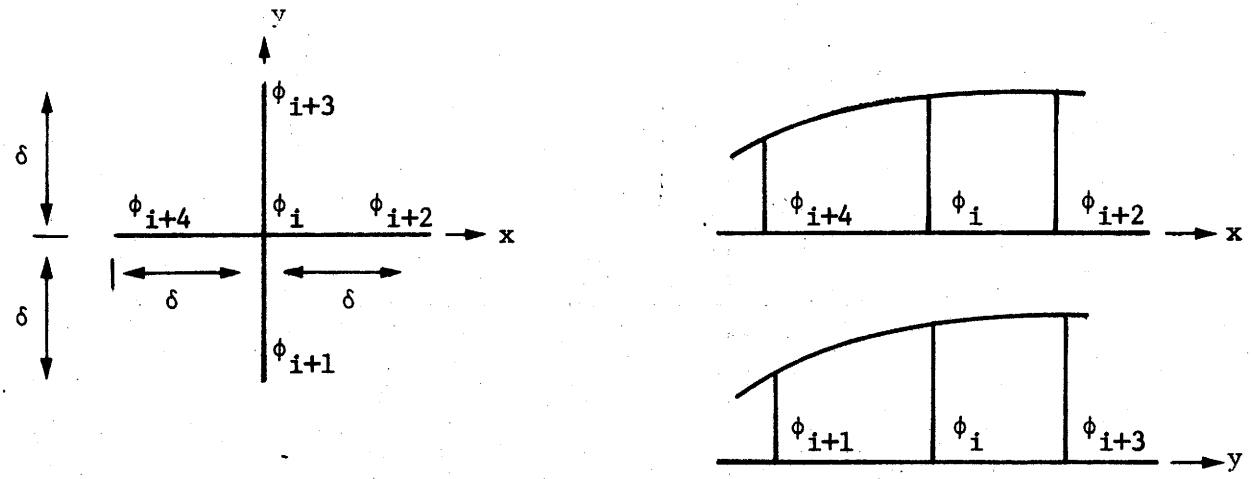

between ϕ_{i+4} and ϕ_i , $\dfrac{\partial\phi}{\partial x} = \dfrac{\phi_i - \phi_{i+4}}{\delta}$

between ϕ_i and ϕ_{i+2} , $\dfrac{\partial\phi}{\partial x} = \dfrac{\phi_{i+2} - \phi_i}{\delta}$

$$\text{at } \phi_i \text{ , } \frac{\partial^2\phi}{\partial x^2} = \frac{\left(\frac{\phi_{i+2} - \phi_i}{\delta}\right) - \left(\frac{\phi_i - \phi_{i+4}}{\delta}\right)}{\delta}$$

$$= \frac{1}{\partial^2}\left(\phi_{i+2} + \phi_{i+4} - 2\phi_i\right)$$

Performing the same operations in the y-direction will yield:

$$\frac{\partial^2\phi}{\partial y^2} = \frac{1}{\partial^2}\left(\phi_{i+3} + \phi_{i+1} - 2\phi_i\right)$$

Equation 1 then becomes:

$$\frac{\partial^2\phi}{\partial x^2} + \frac{\partial^2\phi}{\partial y^2} = \frac{1}{\delta^2}\left(\phi_{i+2} + \phi_{i+4} - 2\phi_i\right) + \frac{1}{\delta^2}\left(\phi_{i+3} + \phi_{i+1} - 2\phi_i\right) = -2G\theta$$

$$\frac{1}{\delta^2}\left(\phi_{i+1} + \phi_{i+2} + \phi_{i+3} + \phi_{i+4} - 4\phi_i\right) = -2G\theta$$

For points along the boundary where the grid pattern for a given point is not complete, the differential equation is evaluated as follows:

Case I:

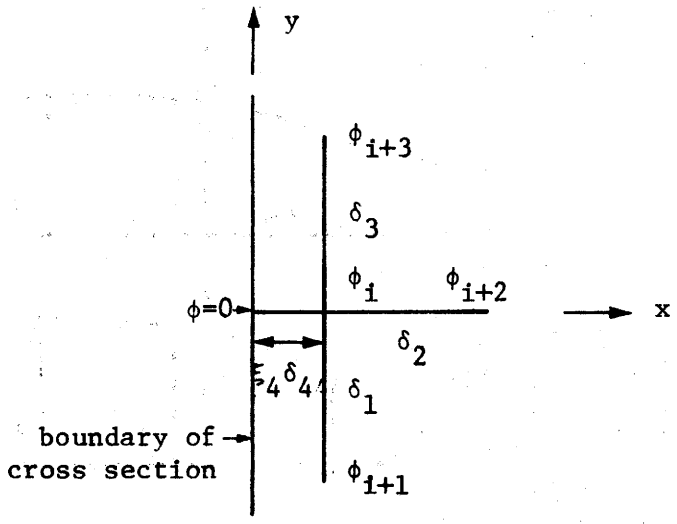

$$\delta_1 = \delta_2 = \delta_3 = \delta_4 = \delta$$

$$\xi_4 = \frac{\delta_4}{\delta}$$

$$\frac{\partial^2\phi}{\partial x^2} = \frac{\dfrac{\phi_{i+2} - \phi_i}{2} - \dfrac{\phi_i - 0}{\xi_4\,\delta}}{\dfrac{\delta + \xi_4\delta}{2}}$$

and $$\frac{\partial^2\phi}{\partial y^2} = \frac{1}{\delta^2}\left(\phi_{i+1} + \phi_{i+3} - 2\phi_i\right)$$

$$\frac{\partial^2\phi}{\partial x^2} + \frac{\partial^2\phi}{\partial y^2} = \frac{2}{\delta^2}\left[\frac{\phi_{i+1}}{2} + \frac{\phi_{i+2}}{1+\xi_4} + \frac{\phi_{i+3}}{2} - \frac{\phi_i}{\xi_4} - \phi_i\right] = -2G\theta$$

Case II:

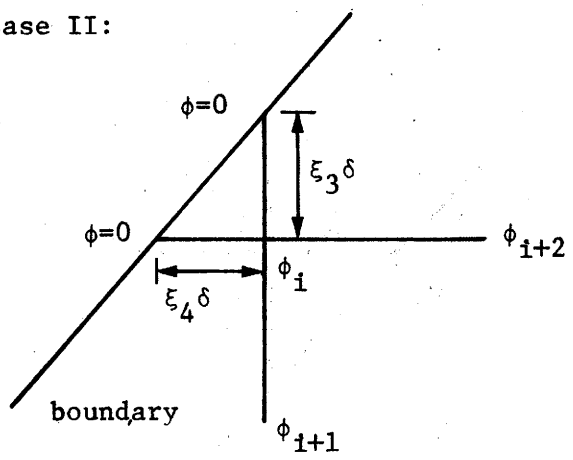

$$\frac{\partial^2\phi}{\partial x^2} = \frac{\dfrac{\phi_{i+2} - \phi_i}{\delta} - \dfrac{\phi_i - 0}{\xi_4\delta}}{\dfrac{\delta + \xi_4\delta}{2}}$$

$$= \frac{2}{\delta^2}\left[\frac{\phi_{i+2}}{1+\xi_4} - \frac{\phi_i}{1+\xi_4} - \frac{\phi_i}{\xi_4(1+\xi_4)}\right]$$

$$\frac{\partial^2\phi}{\partial y^2} = \frac{\dfrac{0-\phi_i}{\xi_3\delta} - \dfrac{\phi_i - \phi_{i+1}}{\delta}}{\dfrac{\xi_3\delta + \delta}{2}}$$

$$= \frac{2}{\delta^2}\left[\frac{-\phi_i}{\xi_3(1+\xi_3)} - \frac{\phi_i}{1+\xi_3} + \frac{\phi_{i+1}}{1+\xi_3}\right]$$

$$\frac{\partial^2\phi}{\partial x^2} + \frac{\partial^2\phi}{\partial y^2} = \frac{2}{\delta^2}\left[\frac{\phi_{i+1}}{1+\xi_3} + \frac{\phi_{i+2}}{1+\xi_4} - \frac{\phi_i}{\xi_3} - \frac{\phi_i}{\xi_4}\right] = -2G\theta$$

Case III:

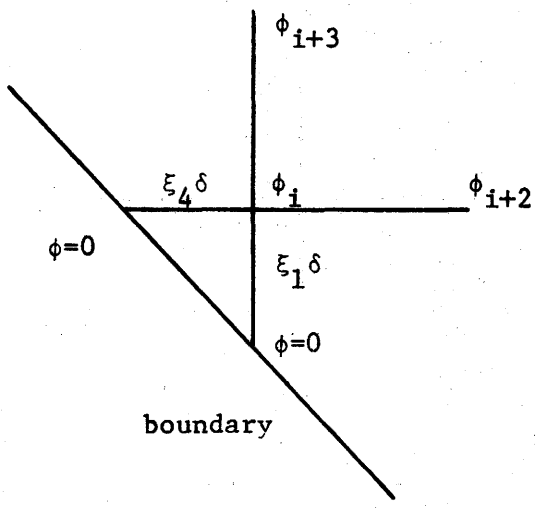

$$\frac{\partial^2\phi}{\partial x^2} = \frac{\dfrac{\phi_{i+2} - \phi_i}{\delta} - \dfrac{\phi_i - 0}{\xi_4\delta}}{\dfrac{\delta(1+\xi_4)}{2}}$$

$$\frac{\partial^2\phi}{\partial y^2} = \frac{\dfrac{\phi_{i+3} - \phi_i}{\delta} - \dfrac{\phi_i - 0}{\xi_1\delta}}{\dfrac{\delta(1+\xi_1)}{2}}$$

$$\frac{\partial^2\phi}{\partial x^2} + \frac{\partial^2\phi}{\partial y^2} = \frac{2}{\delta^2}\left[\frac{\phi_{i+2}}{1+\xi_4} + \frac{\phi_{i+3}}{1+\xi_1} - \frac{\phi_i}{\xi_4} - \frac{\phi_i}{\xi_1}\right] = -2G\theta$$

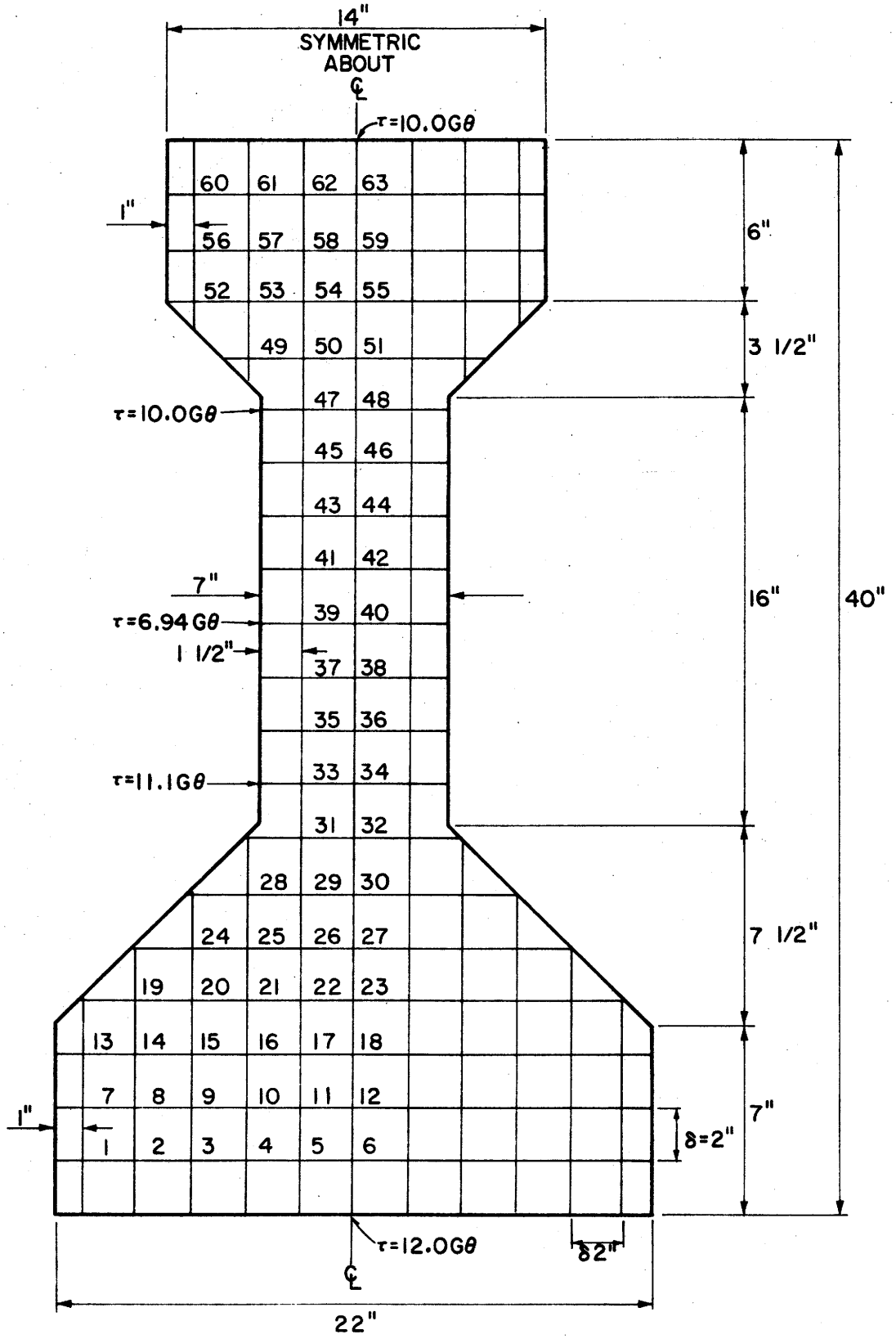

Figure A1: Cross section of THD type C Girder Showing Grid System and Values of Shear Stress at Selected Points.

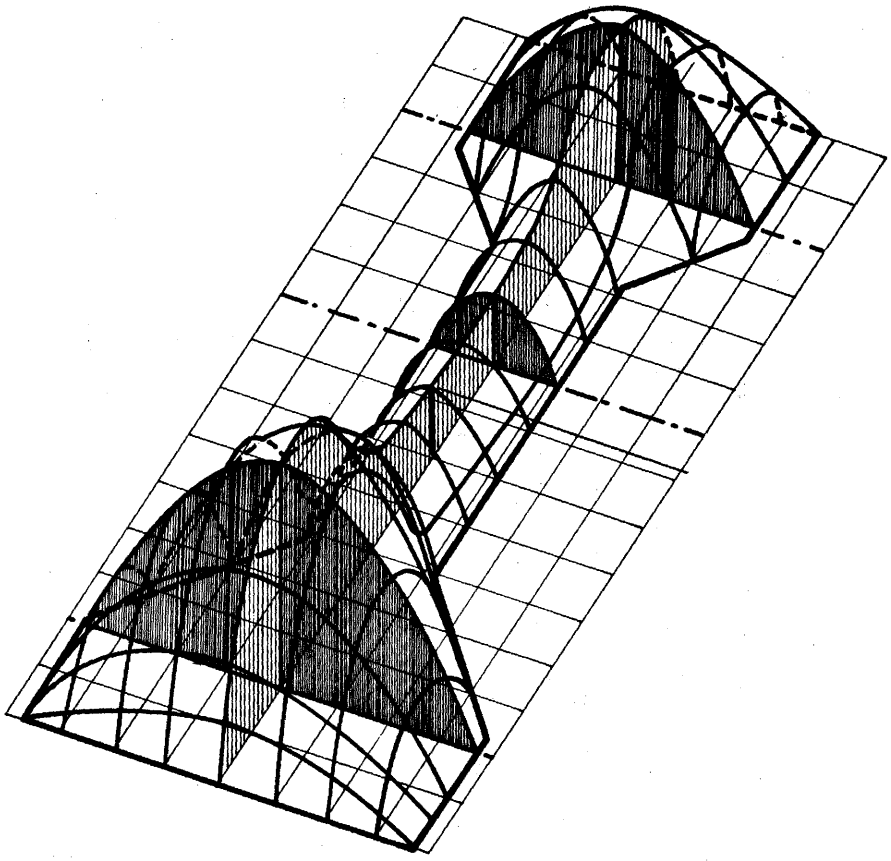

Figure A2. Typical ϕ surface for AASHO girders, after Tamberg.[2]

Table A1

FINITE DIFFERENCE EQUATIONS

FOR THD TYPE C BEAM

Grid point	Equation
1	$4/3\phi_2 + 1\phi_7 - 6\phi_1 = -2G\theta\delta^2$
2	$1\phi_3 + 1\phi_8 + 1\phi_1 - 4\phi_2 = -2G\theta\delta^2$
3	$1\phi_4 + 1\phi_9 + 1\phi_2 - 4\phi_3 = -2G\theta\delta^2$
4	$1\phi_5 + 1\phi_{10} + 1\phi_3 - 4\phi_4 = -2G\theta\delta^2$
5	$1\phi_6 + 1\phi_{11} + 1\phi_4 - 4\phi_5 = -2G\theta\delta^2$
6	$2\phi_5 + 1\phi_{12} - 4\phi_6 = -2G\theta\delta^2$
7	$4/3\phi_8 + 1\phi_{13} + 1\phi_1 - 6\phi_7 = -2G\theta\delta^2$
8	$1\phi_9 + 1\phi_{14} + 1\phi_7 + 1\phi_2 - 4\phi_8 = -2G\theta\delta^2$
9	$1\phi_{10} + 1\phi_{15} + 1\phi_8 + 1\phi_3 - 4\phi_9 = -2G\theta\delta^2$
10	$1\phi_{11} + 1\phi_{16} + 1\phi_9 + 1\phi_4 - 4\phi_{10} = -2G\theta\delta^2$
11	$1\phi_{12} + 1\phi_{17} + 1\phi_{10} + 1\phi_5 - 4\phi_{11} = -2G\theta\delta^2$
12	$2\phi_{11} + 1\phi_{18} + 1\phi_6 - 4\phi_{12} = -2G\theta\delta^2$
13	$4/3\phi_{14} + 1\phi_7 - 6\phi_{13} = -2G\theta\delta^2$
14	$1\phi_{15} + 1\phi_{19} + 1\phi_{13} + 1\phi_8 - 4\phi_{14} = -2G\theta\delta^2$
15	$1\phi_{16} + 1\phi_{20} + 1\phi_{14} + 1\phi_9 - 4\phi_{15} = -2G\theta\delta^2$
16	$1\phi_{17} + 1\phi_{21} + 1\phi_{15} + 1\phi_{10} - 4\phi_{16} = -2G\theta\delta^2$
17	$1\phi_{18} + 1\phi_{22} + 1\phi_{16} + 1\phi_{11} - 4\phi_{17} = -2G\theta\delta^2$
18	$2\phi_{17} + 1\phi_{23} + 1\phi_{12} - 4\phi_{18} = -2G\theta\delta^2$

Grid point	Equation
19	$1\phi_{14} + 1\phi_{20} - 4\phi_{19} = -2G\theta\delta^2$
20	$1\phi_{21} + 1\phi_{24} + 1\phi_{19} + 1\phi_{15} - 4\phi_{20} = -2G\theta\delta^2$
21	$1\phi_{22} + 1\phi_{25} + 1\phi_{20} + 1\phi_{16} - 4\phi_{21} = -2G\theta\delta^2$
22	$1\phi_{23} + 1\phi_{26} + 1\phi_{21} + 1\phi_{17} - 4\phi_{22} = -2G\theta\delta^2$
23	$2\phi_{22} + 1\phi_{27} + 1\phi_{18} - 4\phi_{23} = -2G\theta\delta^2$
24	$1\phi_{20} + 1\phi_{25} - 4\phi_{24} = -2G\theta\delta^2$
25	$1\phi_{26} + 1\phi_{28} + 1\phi_{24} + 1\phi_{21} - 4\phi_{25} = -2G\theta\delta^2$
26	$1\phi_{27} + 1\phi_{29} + 1\phi_{25} + 1\phi_{22} - 4\phi_{26} = -2G\theta\delta^2$
27	$2\phi_{26} + 1\phi_{30} + 1\phi_{23} - 4\phi_{27} = -2G\theta\delta^2$
28	$1\phi_{25} + 1\phi_{29} - 4\phi_{28} = -2G\theta\delta^2$
29	$1\phi_{30} + 1\phi_{31} + 1\phi_{28} + 1\phi_{26} - 4\phi_{29} = -2G\theta\delta^2$
30	$2\phi_{29} + 1\phi_{32} + 1\phi_{27} - 4\phi_{30} = -2G\theta\delta^2$
31	$1\phi_{29} + 1\phi_{32} + 1\phi_{33} - 4\phi_{31} = -2G\theta\delta^2$
32	$2\phi_{31} + 1\phi_{34} + 1\phi_{30} - 4\phi_{32} = -2G\theta\delta^2$
33	$8/7\phi_{34} - 14/3\phi_{33} + 1\phi_{35} + 1\phi_{31} = -2G\theta\delta^2$
34	$2\phi_{33} + 1\phi_{36} + 1\phi_{32} - 4\phi_{34} = -2G\theta\delta^2$
35	$8/7\phi_{36} - 14/3\phi_{35} + 1\phi_{37} + 1\phi_{33} = -2G\theta\delta^2$
36	$2\phi_{35} + 1\phi_{38} + 1\phi_{34} - 4\phi_{36} = -2G\theta\delta^2$
37	$8/7\phi_{38} - 14/3\phi_{37} + 1\phi_{39} + 1\phi_{35} = -2G\theta\delta^2$
38	$2\phi_{37} + 1\phi_{40} + 1\phi_{36} - 4\phi_{38} = -2G\theta\delta^2$
39	$8/7\phi_{40} - 14/3\phi_{39} + 1\phi_{41} + 1\phi_{37} = -2G\theta\delta^2$
40	$2\phi_{39} + 1\phi_{42} + 1\phi_{38} - 4\phi_{40} = -2G\theta\delta^2$
41	$8/7\phi_{42} - 14/3\phi_{41} + 1\phi_{43} + 1\phi_{39} = -2G\theta\delta^2$

Grid point	Equation
42	$2\phi_{41} + 1\phi_{44} + 1\phi_{40} - 4\phi_{42} = -2G\theta\delta^2$
43	$8/7\phi_{44} - 14/3\phi_{43} + 1\phi_{45} + 1\phi_{41} = -2G\theta\delta^2$
44	$2\phi_{43} + 1\phi_{46} + 1\phi_{42} - 4\phi_{44} = -2G\theta\delta^2$
45	$8/7\phi_{46} - 14/3\phi_{45} + 1\phi_{47} + 1\phi_{43} = -2G\theta\delta^2$
46	$2\phi_{45} + 1\phi_{48} + 1\phi_{44} - 4\phi_{46} = -2G\theta\delta^2$
47	$8/7\phi_{48} - 14/3\phi_{47} + 1\phi_{50} + 1\phi_{45} = -2G\theta\delta^2$
48	$2\phi_{47} + 1\phi_{51} + 1\phi_{46} - 4\phi_{48} = -2G\theta\delta^2$
49	$4/3\phi_{50} + 4/3\phi_{53} - 8\phi_{49} = -2G\theta\delta^2$
50	$1\phi_{51} + 1\phi_{54} + 1\phi_{49} + 1\phi_{47} - 4\phi_{50} = -2G\theta\delta^2$
51	$2\phi_{50} + 1\phi_{55} + 1\phi_{48} - 4\phi_{51} = -2G\theta\delta^2$
52	$4/3\phi_{53} + 4/3\phi_{56} - 8\phi_{52} = -2G\theta\delta^2$
53	$1\phi_{54} + 1\phi_{57} + 1\phi_{52} + 1\phi_{49} - 4\phi_{53} = -2G\theta\delta^2$
54	$1\phi_{55} + 1\phi_{58} + 1\phi_{53} + 1\phi_{50} - 4\phi_{54} = -2G\theta\delta^2$
55	$2\phi_{54} + 1\phi_{59} + 1\phi_{51} - 4\phi_{55} = -2G\theta\delta^2$
56	$4/3\phi_{57} + 1\phi_{60} + 1\phi_{52} - 6\phi_{56} = -2G\theta\delta^2$
57	$1\phi_{58} + 1\phi_{61} + 1\phi_{56} + 1\phi_{53} - 4\phi_{57} = -2G\theta\delta^2$
58	$1\phi_{59} + 1\phi_{62} + 1\phi_{57} + 1\phi_{54} - 4\phi_{58} = -2G\theta\delta^2$
59	$2\phi_{58} + 1\phi_{63} + 1\phi_{55} - 4\phi_{59} = -2G\theta\delta^2$
60	$4/3\phi_{61} + 1\phi_{56} - 6\phi_{60} = -2G\theta\delta^2$
61	$1\phi_{62} + 1\phi_{60} + 1\phi_{57} - 4\phi_{61} = -2G\theta\delta^2$
62	$1\phi_{63} + 1\phi_{61} + 1\phi_{58} - 4\phi_{62} = -2G\theta\delta^2$
63	$2\phi_{62} + 1\phi_{59} - 4\phi_{63} = -2G\theta\delta^2$

This system of equations can be expressed in matrix notation as:

$$[K]\ \{\phi\} = \{-2G\theta\}$$

or $$\{\phi\} = [K]^{-1}\ \{-2G\theta\}$$

In order to solve this equation one must invert the coefficient matrix, [K], and multiply that inverse by the column matrix, $\{-2G\theta\}$. For these operations, a computer program is used. The resulting values of ϕ are tabulated in table A3.

Table A2

MATRIX OF COEFFICIENTS

	1	2	3	4	5	6	7	8	9	10	11	12	13	14	15	16	17	18	19	20
1	-6	1.33					1													
2	1	-4	1					1												
3		1	-4	1					1											
4			1	-4	1					1										
5				1	-4	1					1									
6					2	-4						1								
7	1						-6	1.33					1							
8		1					1	-4	1					1						
9			1					1	-4	1					1					
10				1					1	-4	1					1				
11					1					1	-4	1					1			
12						1					2	-4						1		
13							1						-6	1.33						
14								1					1	-4	1				1	
15									1					1	-4	1				1

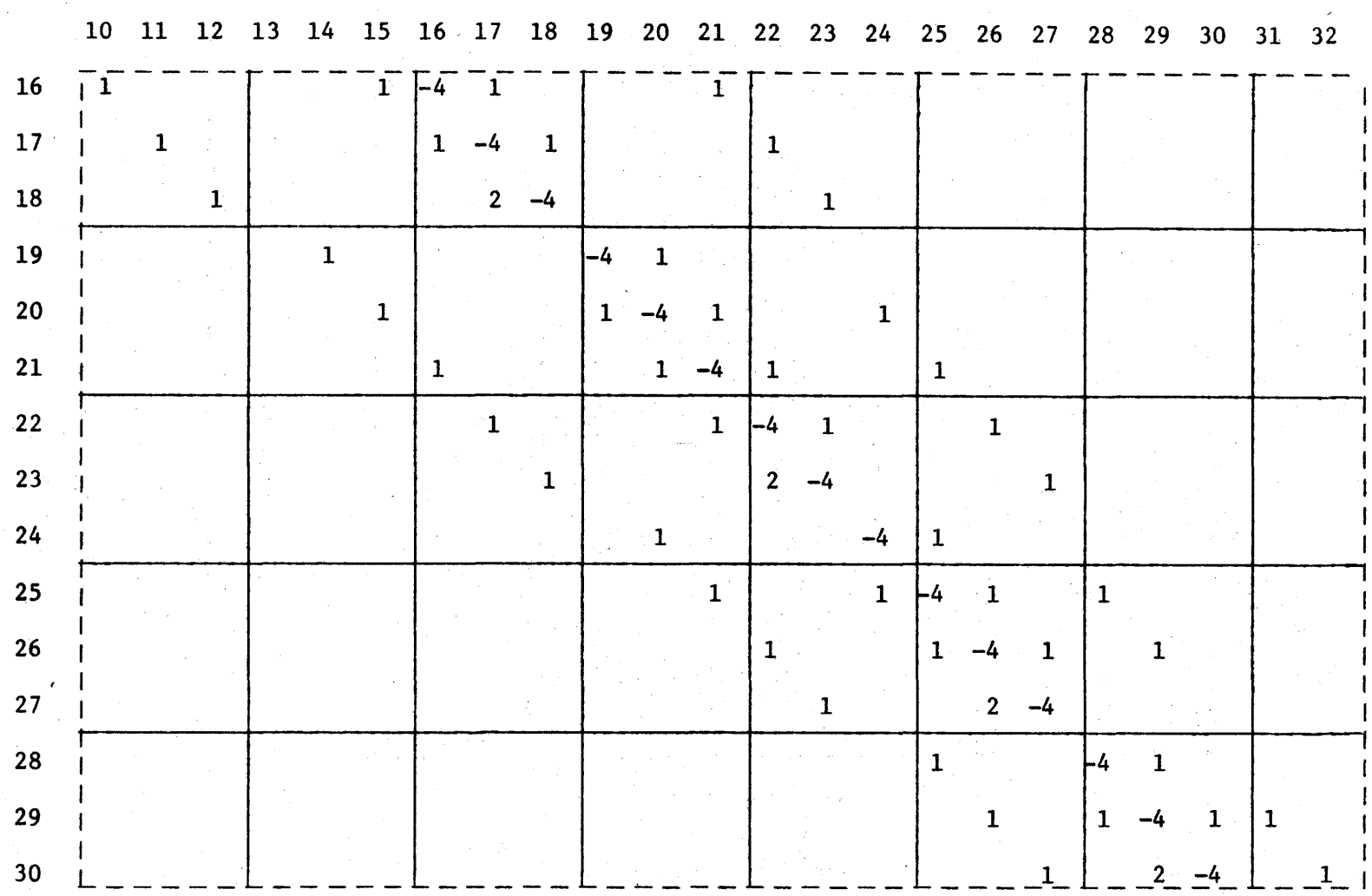
10 11 12 13 14 15 16 17 18 19 20 21 22 23 24 25 26 27 28 29 30 31 32
16 1 1 -4 1 1
17 1 1 -4 1 1
18 1 2 -4 1
19 1 -4 1
20 1 1 -4 1 1
21 1 1 -4 1 1
22 1 1 -4 1 1
23 1 2 -4 1
24 1 1 -4
25 1 1 -4 1 1
26 1 1 -4 1 1
27 1 2 -4
28 1 -4 1
29 1 1 -4 1 1
30 2 -4 1

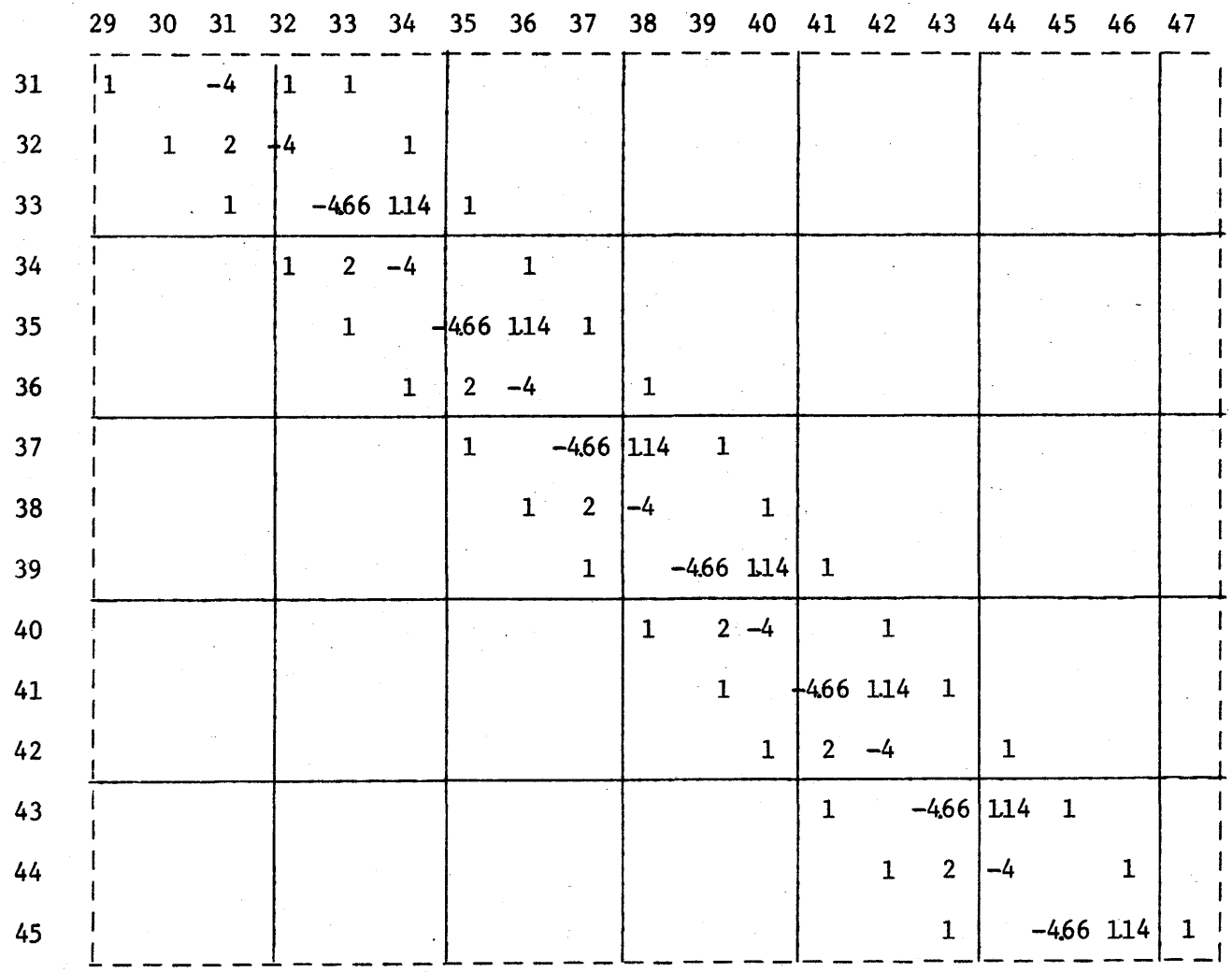
29 30 31 32 33 34 35 36 37 38 39 40 41 42 43 44 45 46 47
31 1 -4 1 1
32 1 2 -4 1
33 1 -4.66 1.14 1
34 1 2 -4 1
35 1 -4.66 1.14 1
36 1 2 -4 1
37 1 -4.66 1.14 1
38 1 2 -4 1
39 1 -4.66 1.14 1
40 1 2 -4 1
41 1 -4.66 1.14 1
42 1 2 -4 1
43 1 -4.66 1.14 1
44 1 2 -4 1
45 1 -4.66 1.14 1

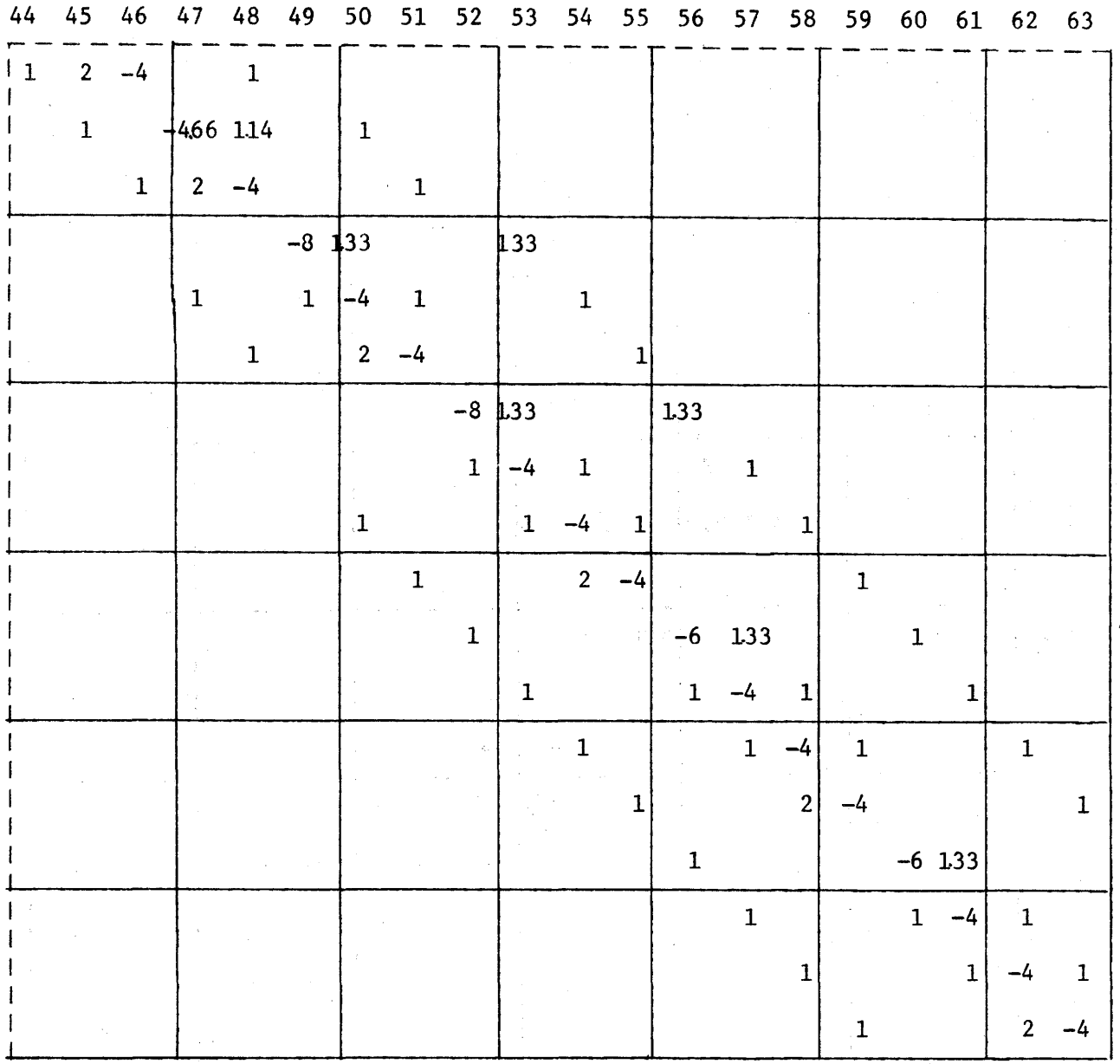
44 45 46 47 48 49 50 51 52 53 54 55 56 57 58 59 60 61 62 63
46 1 2 -4 1
47 1 -4 6 6 1 1 4 1
48 1 2 -4 1
49 -8 1 3 3 1 3 3
50 1 1 -4 1 1
51 1 2 -4 1
52 -8 1 3 3 1 3 3
53 1 -4 1 1
54 1 1 -4 1 1
55 1 2 -4 1
56 1 -6 1 3 3 1
57 1 1 -4 1 1
58 1 1 -4 1 1 1
59 1 -4 2 1
60 1 -6 1 3 3
61 1 1 -4 1
62 1 1 -4 1
63 1 2 -4

Table A3 VALUES FOR ϕ AT THE VARIOUS GRID P0INTS IN A THD TYPE C PRESTRESSED CONCRETE GIRDER

Grid Point	Value of ϕ	Grid Point	Value of ϕ	Grid Point	Value of ϕ	Grid Point	Value of ϕ
1*	4.97GΘ	17	36.33	33	11.35	49	5.66
2	11.16	18	37.68	34	16.61	50	15.51
3	15.01	19	12.00	35	9.50	51	18.88
4	17.47	20	22.76	36	14.18	52	4.02
5	18.87	21	31.18	37	8.79	53	12.43
6	19.34	22	36.59	38	13.12	54	18.68
7	6.92	23	38.45	39	8.54	55	20.90
8	16.68	24	13.94	40	12.72	56	5.70
9	23.40	25	25.00	41	8.51	57	13.36
10	27.98	26	32.39	42	12.68	58	17.86
11	30.70	27	34.96	43	8.70	59	19.37
12	31.60	28	14.50	44	12.96	60	4.38
13	6.32	29	24.99	45	9.28	61	9.45
14	17.23	30	28.62	46	13.78	62	12.04
15	25.94	31	16.47	47	10.84	63	12.87
16	32.36	32	21.54	48	15.59		

*See Figure A1 for grid point locations. Values of ϕ are symmetric about the vertical centerline of the cross-section.

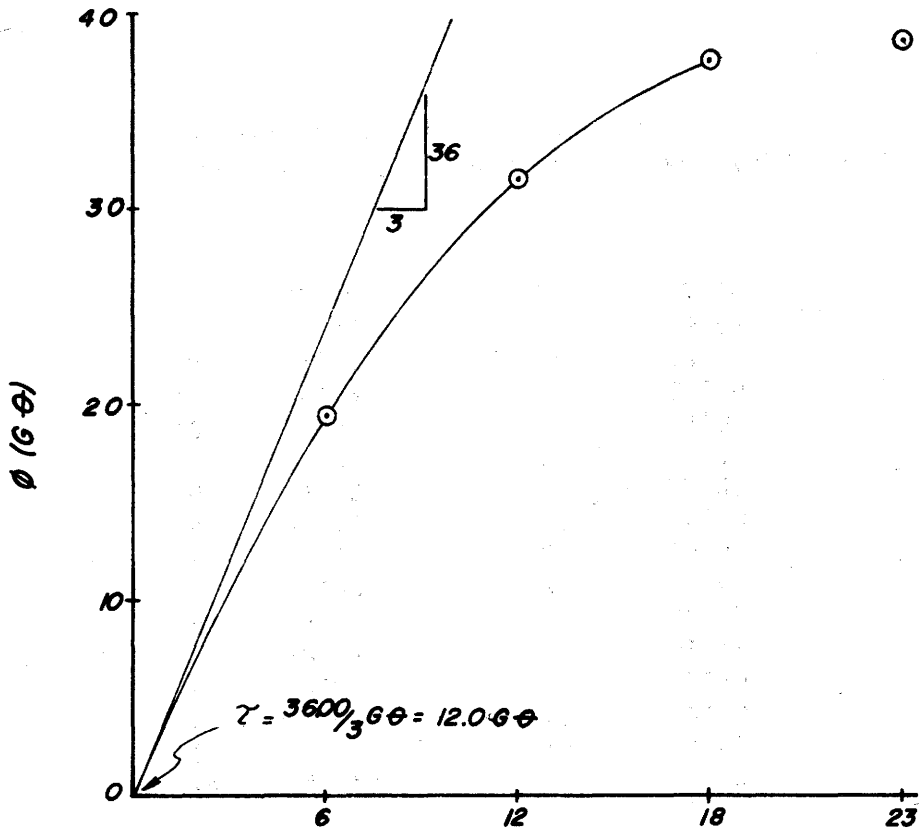

Figure A3a

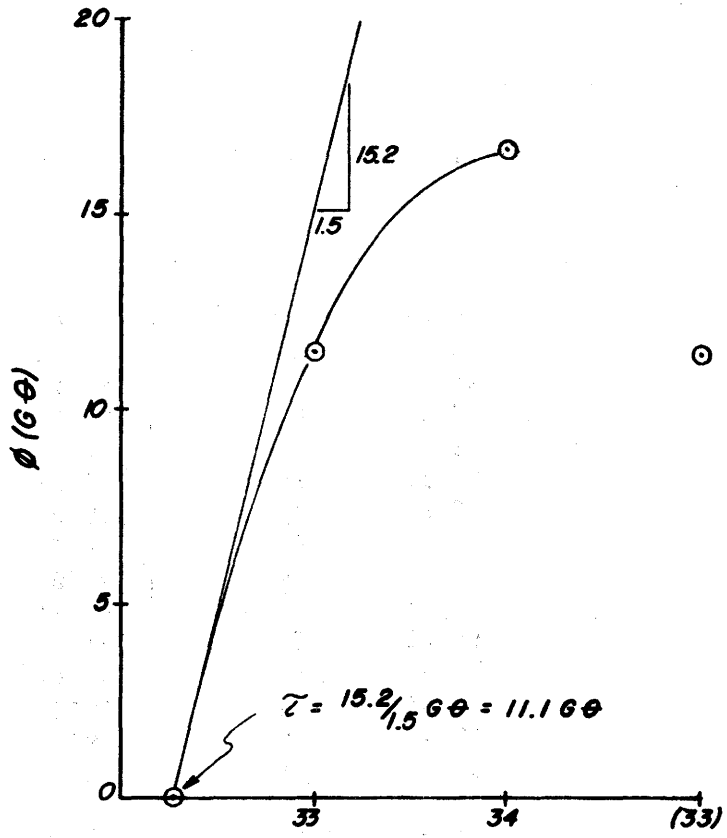

Figure A3b

Figure A3: Cross sections of stress function surface for evaluation of shear stresses.

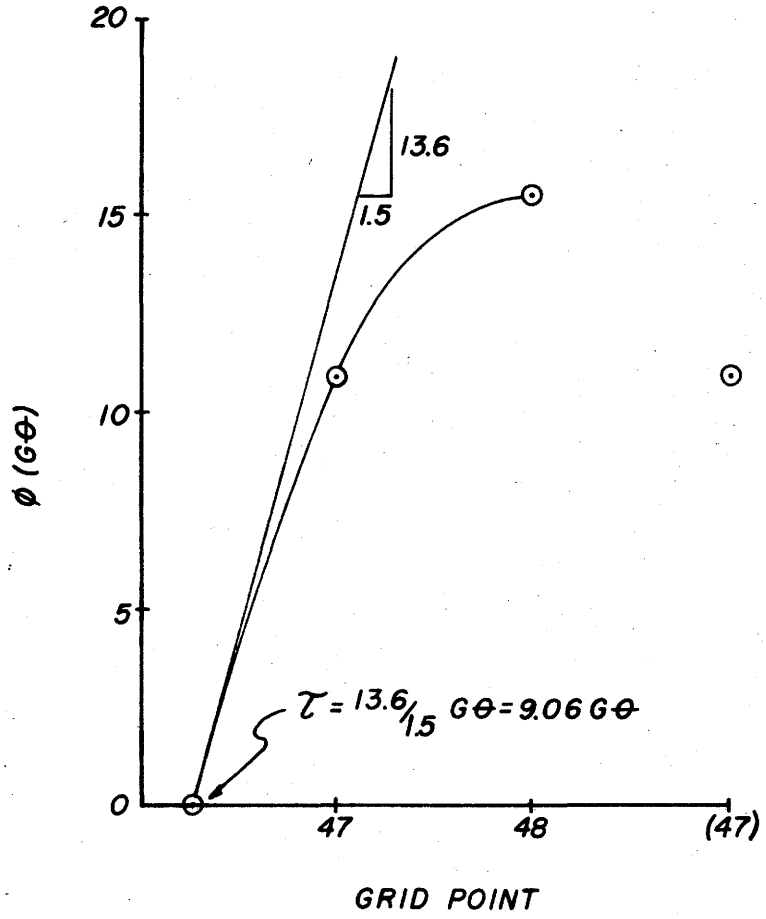

Figure A3c.

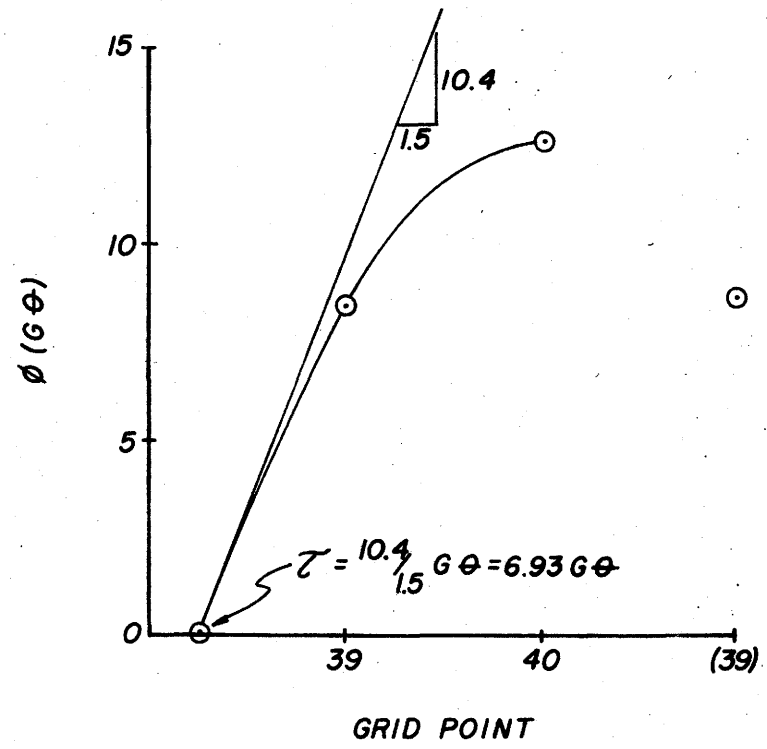

Figure A3d.

At any given point on the cross section, the torsional shear stress in any direction is equal to the slope of the ϕ surface in a perpendicular direction, i.e. $\frac{\partial \phi}{\partial x} = \tau_y$ and $\frac{\partial \phi}{\partial y} = \tau_x$. Values of shear stress on the surface can be obtained by plotting the cross section of the ϕ surface along a grid line that is perpendicular to the surface at the point of interest and graphically measuring its slope of the edge of the cross section of the beam. Values of shearing stress obtained in this manner are listed in Figure A1.

The magnitude of the torque transmitted is equal to twice the volume under the ϕ surface, i.e.

$$T = 2 \int_{\text{area of x-sect.}} \phi dxdy$$

This integral can best be evaluated using numerical techniques since no equation describing the ϕ surface has been written and would be difficult if not impossible to obtain. Since the torque, T, is also equal to $KG\theta$, K can be evaluated as follows:

$$K = \frac{2 \int_{\text{area}} \phi dxdy}{G\theta}$$

$$\text{or} \quad K = \frac{2 \text{ (vol. under } \phi)}{G\theta}$$

Evaluation of $\int_{\text{area}} \phi dxdy$ using Simpson's rule yields the volume under the surface to be 7308 $G\theta$ in.^{3} and K is found to be 14,600 in.^{4}.

APPENDIX B

APPENDIX B

Calculation of Stresses Induced During Construction

The following is a method of approach for calculating the stresses induced by cantilevered forms and other torque-producing loads during construction.

A typical type of form for the overhanging deck is illustrated in Figure B1. The loads due to the forms, plastic deck, and any other torque-producing loads can be represented as in Figures B2 and B3.

DIAPHRAGMS CURED PRIOR TO PLACING SLAB.
SLAB CONCRETE PLACED BETWEEN INSIDE
& OUTSIDE BEAMS PRIOR TO PLACEMENT
IN OVERHANG.

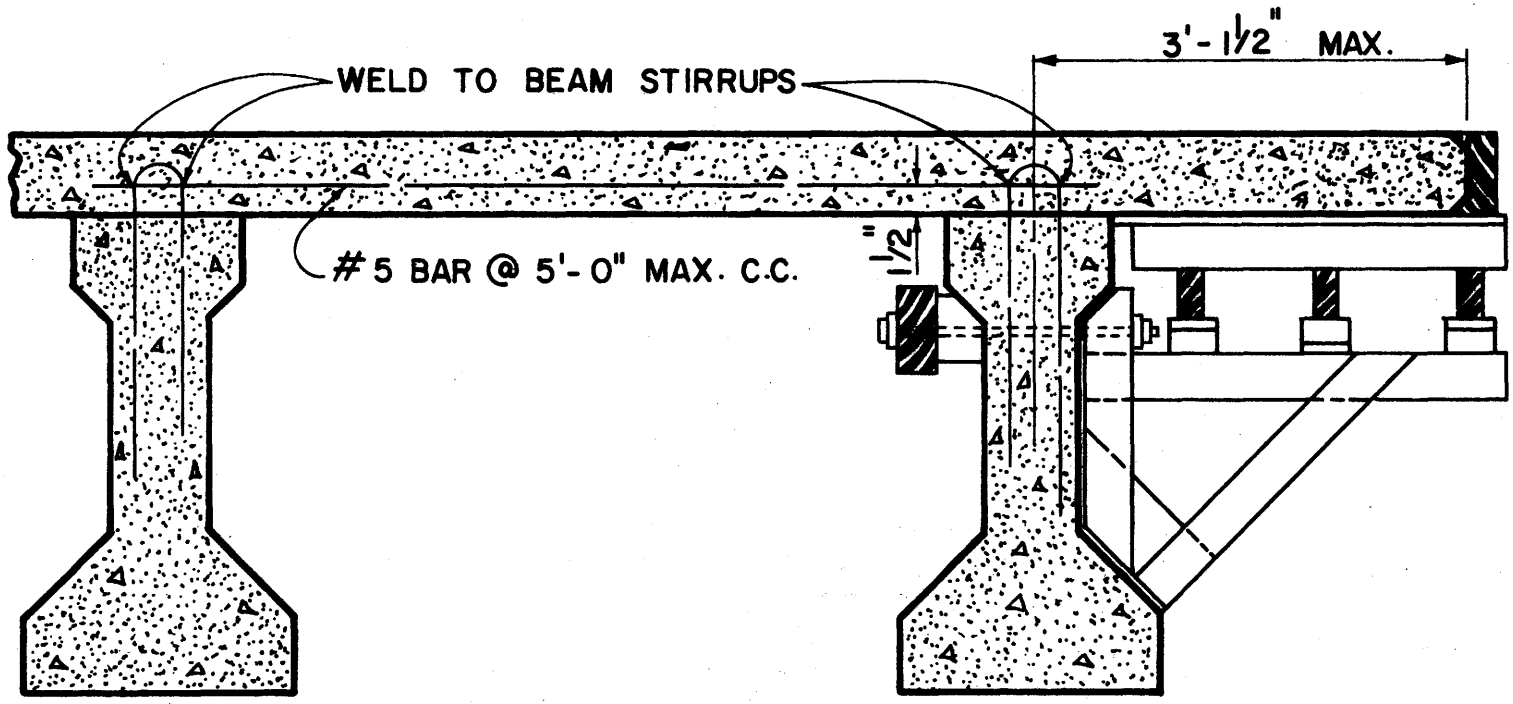

OVERHANG SUPPORT
SHOWING USE OF BRACKETS FOR STANDARD OVERHANG

Figure B1.

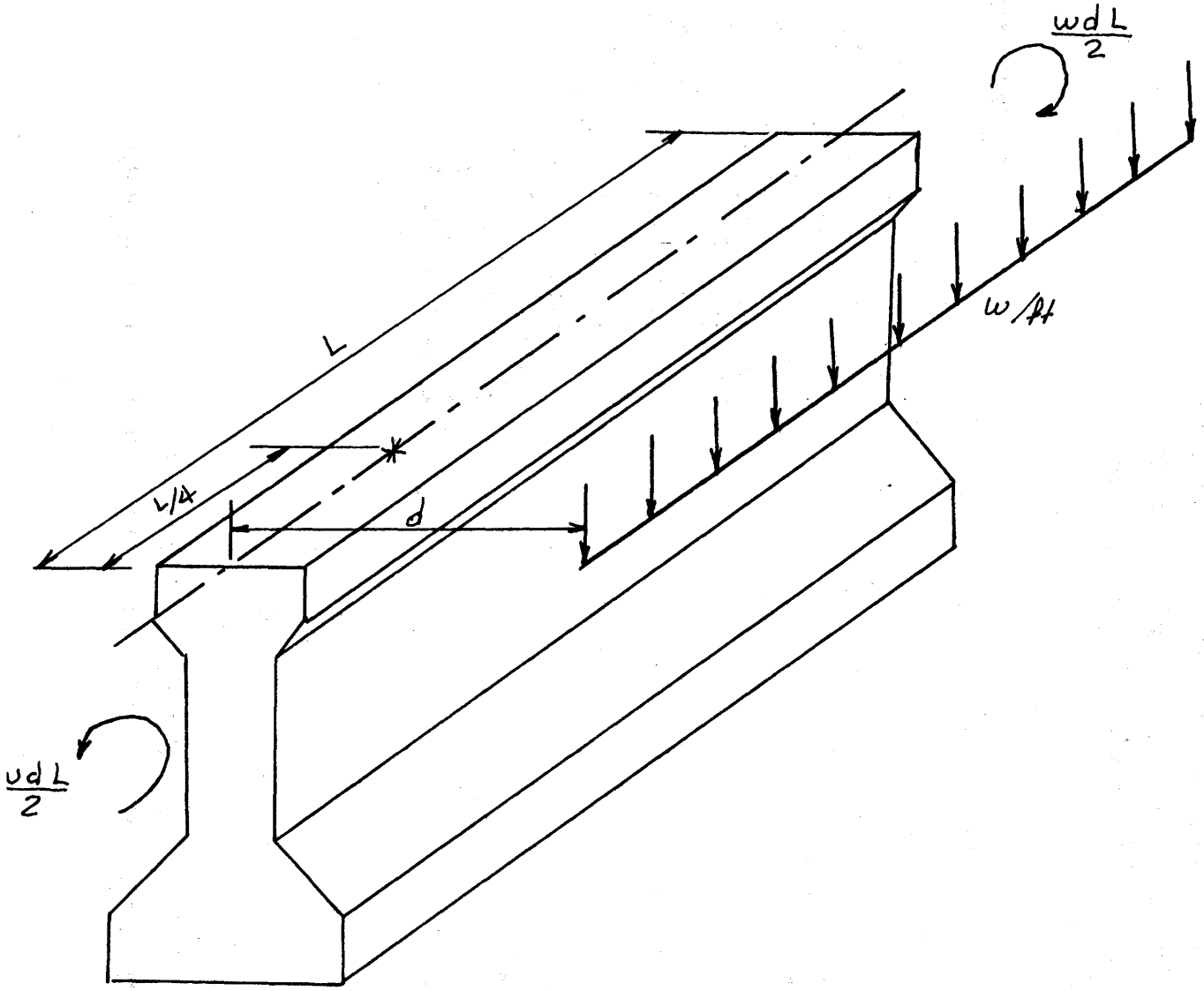

Figure B2.

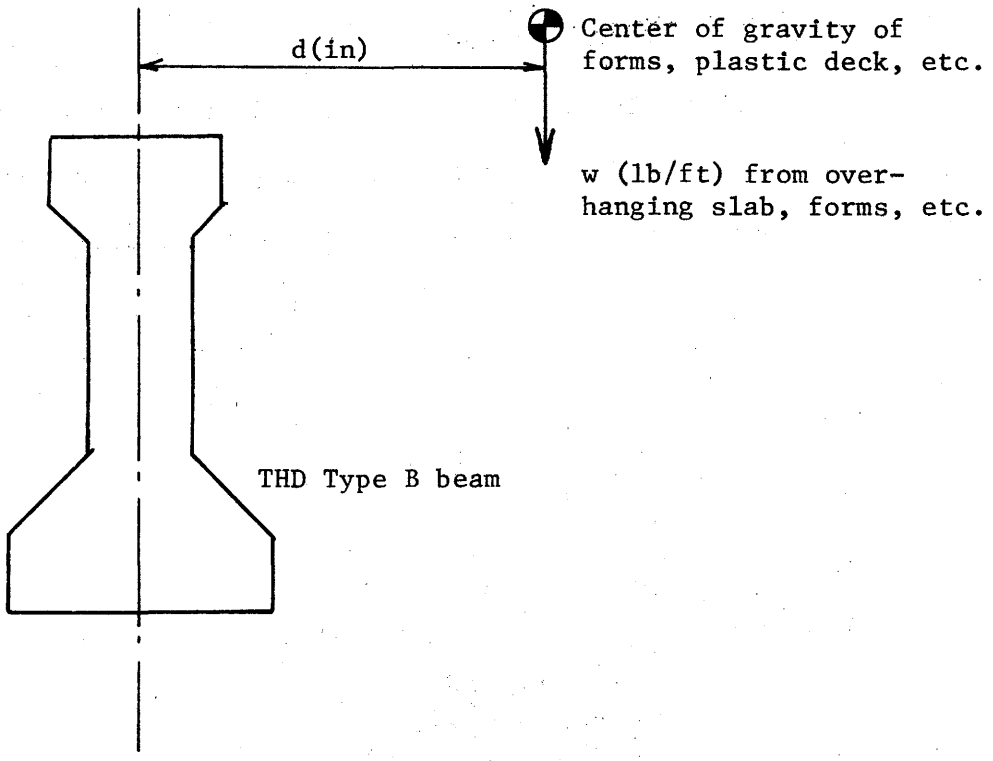

w - weight of overhanging parts in pounds per linear foot of beam

d - distance in inches from center line of beam to center of gravity of load, w.

Figure B3: Cross-section of beam and torque producing load.

Assume the beam fixed against torsional rotation but simply supported for flexural loading on both ends and uniformly loaded with an overhanging load. Neglect interior diaphragms. The torsional loading per foot of beam is wd and the diagram of the torsional load is:

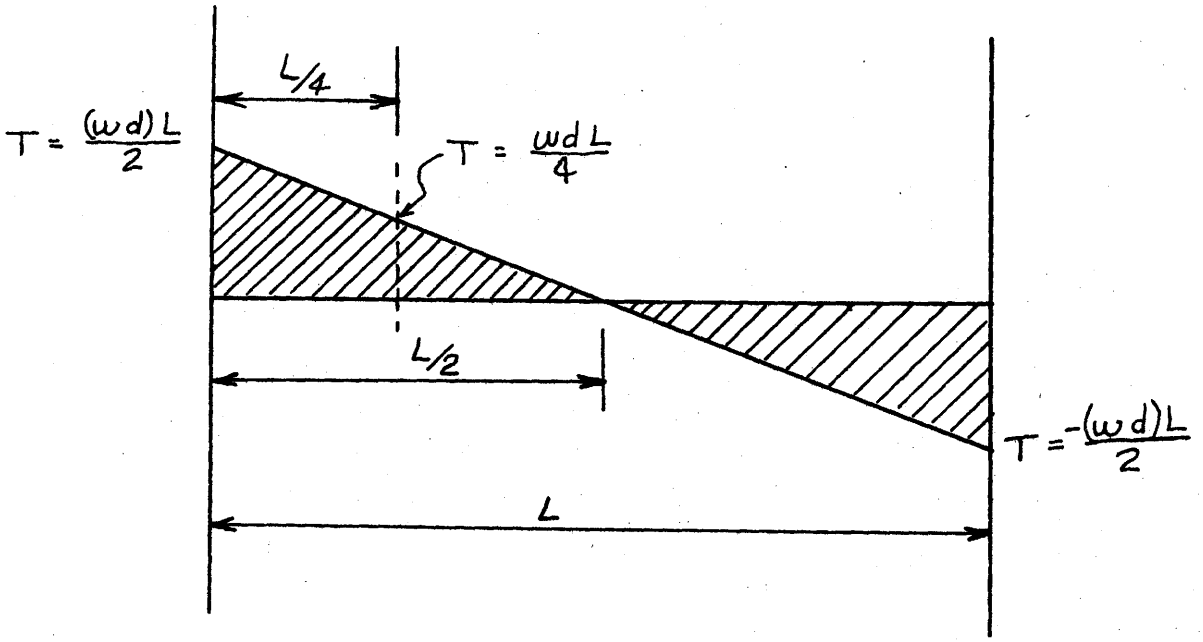

Torsion Diagram
Figure B4.

Maximum torque occurs at each end of the beam and is $\frac{(wd)L}{2}$ in-lbs.

This same loading also causes bending of the beam. Assuming the beam to be simply supported on each end, the moment diagram is:

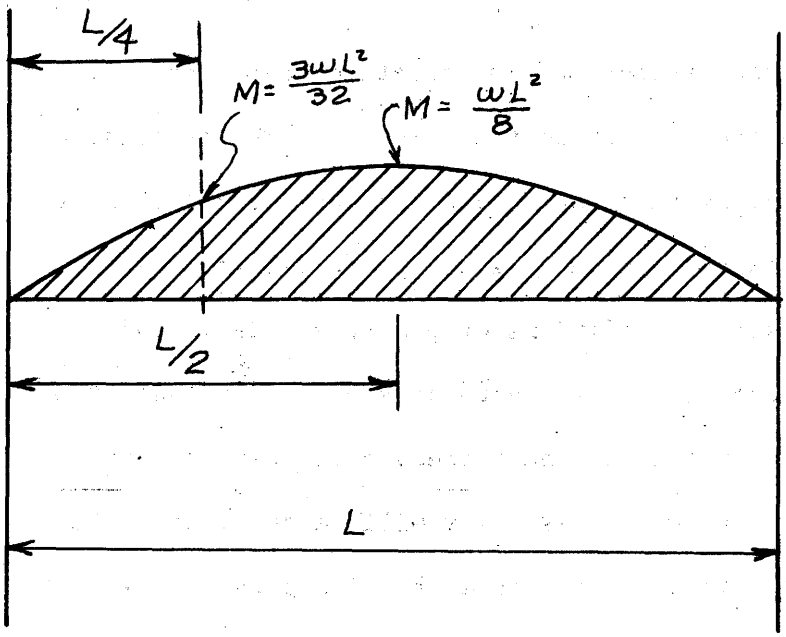

Bending Moment Diagram
Figure B5.

The shear diagram for this loading is:

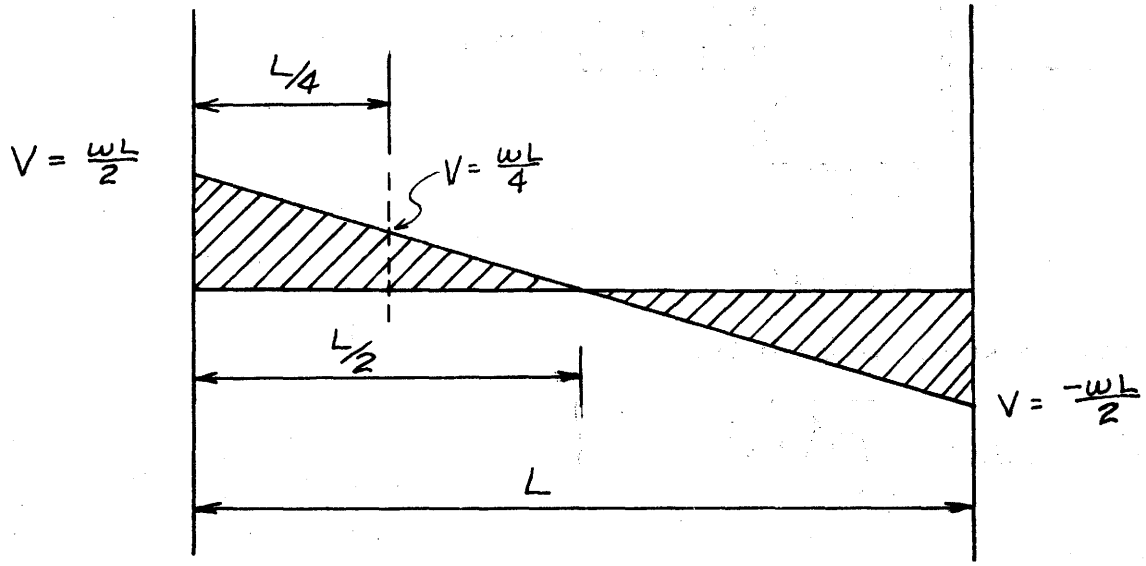

Shear Diagram
Figure B6.

The particular cross section and the point on that cross section that is most critical can not be located directly. The stresses at a number of points must be calculated to determine the location of the point which will experience the highest principal tensile stresses for a given set of conditions of prestress, deal load, torque and flexural loadings. For the purpose of this illustration, a single point will be chosen and the procedure for determining the principal tensile stress at this point will be outlined. The point chosen is in the middle of the top flange at a distance of L/4 from the end of the beam. The flexural stress at this point is f_b, the prestress plus dead load stress is f_{p+dl}, the torsional stress is τ, and the flexural shear is zero. These stresses are illustrated on the following stress block.

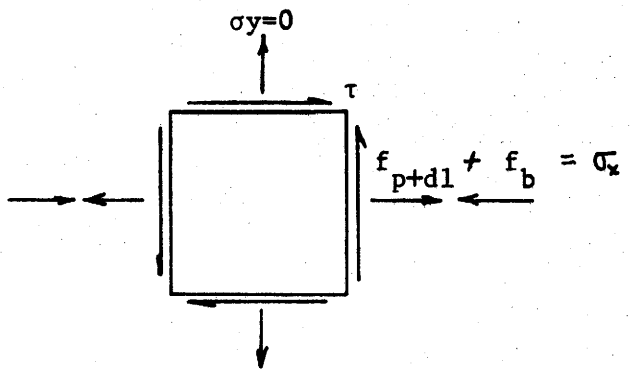

Figure B7.

The principal tensile stress is given by:

$$\sigma_1 = \frac{\sigma_x}{2} + \sqrt{\left(\frac{\sigma_x}{2}\right)^2 + \tau^2}$$

APPENDIX C

APPENDIX C

Procedure for Calculating Principal Stresses

The principal stresses are calculated using the basic strength of materials relationships for plane stress:

$$\sigma_{1,2} = \frac{\sigma_x + \sigma_y}{2} \pm \sqrt{\left(\frac{\sigma_x - \sigma_y}{2}\right)^2 + \tau_{xy}^2} \quad \text{- - - - - - - - - - (C1)}$$

and

$$\text{Tan } 2\theta_p = \frac{\tau_{xy}}{(\sigma_x - \sigma_y)/2} \quad \text{- - - - - - - - - - - - - - - - - - - (C2)}$$

where: $\sigma_{1,2}$ = principal normal stresses, psi

σ_x, σ_y = normal stresses in x and y - direction, psi

τ_{xy} = shearing stress, psi

θ_p = angle between x - y directions and the directions of principal stresses, degrees.

The stress block is as follows:

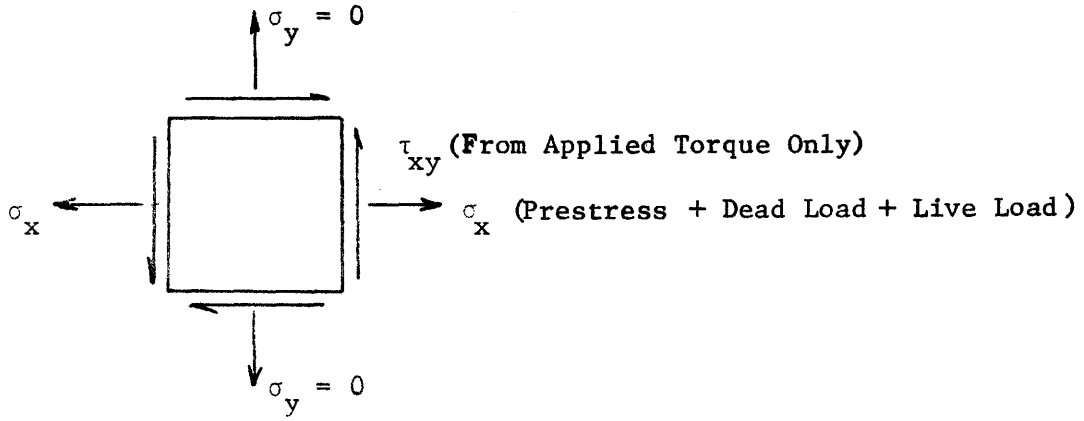

with $\sigma_y = 0$, equation 1 becomes:

$$\sigma_{1,2} = \frac{\sigma_x}{2} \pm \sqrt{\left(\frac{\sigma_x}{2}\right)^2 + \tau_{xy}^2} \quad \text{- - - - - - - - - - - - - - - - (C3)}$$

σ_x is the normal stress at the point in question created by prestress plus dead load stress. These stresses for the normal weight and lightweight girders are given in the following figure.

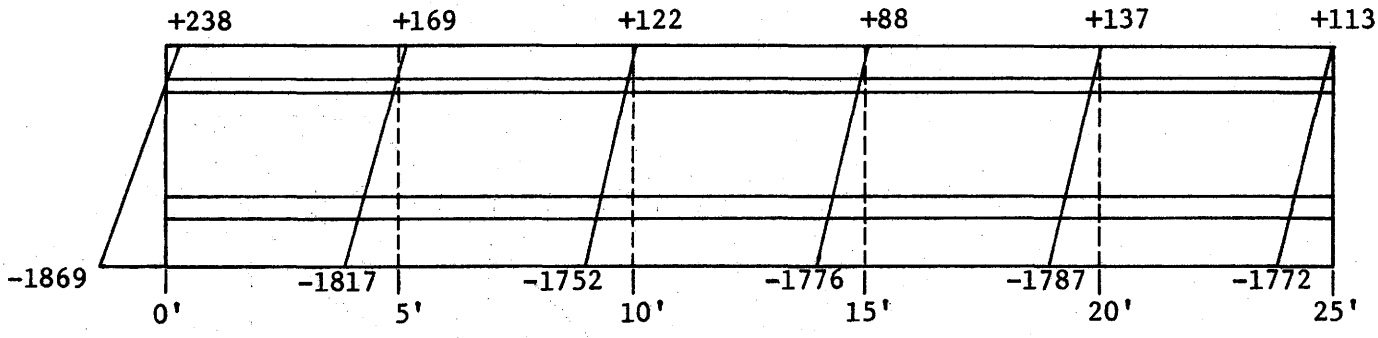

Figure C1: Stresses due to dead load plus prestress for normal weight girder tested in this study.

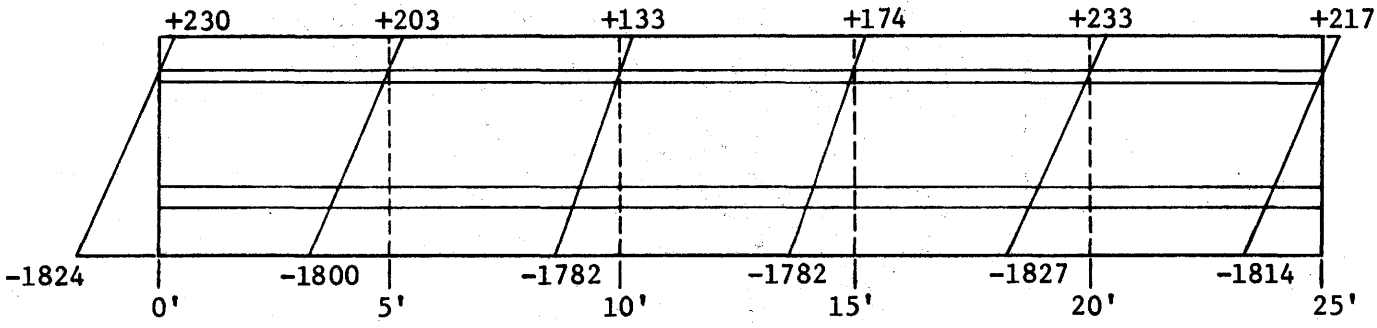

Figure C2: Stresses due to dead load plus prestress for lightweight girder.

The states of stress at selected points on the girder are calculated as follows:

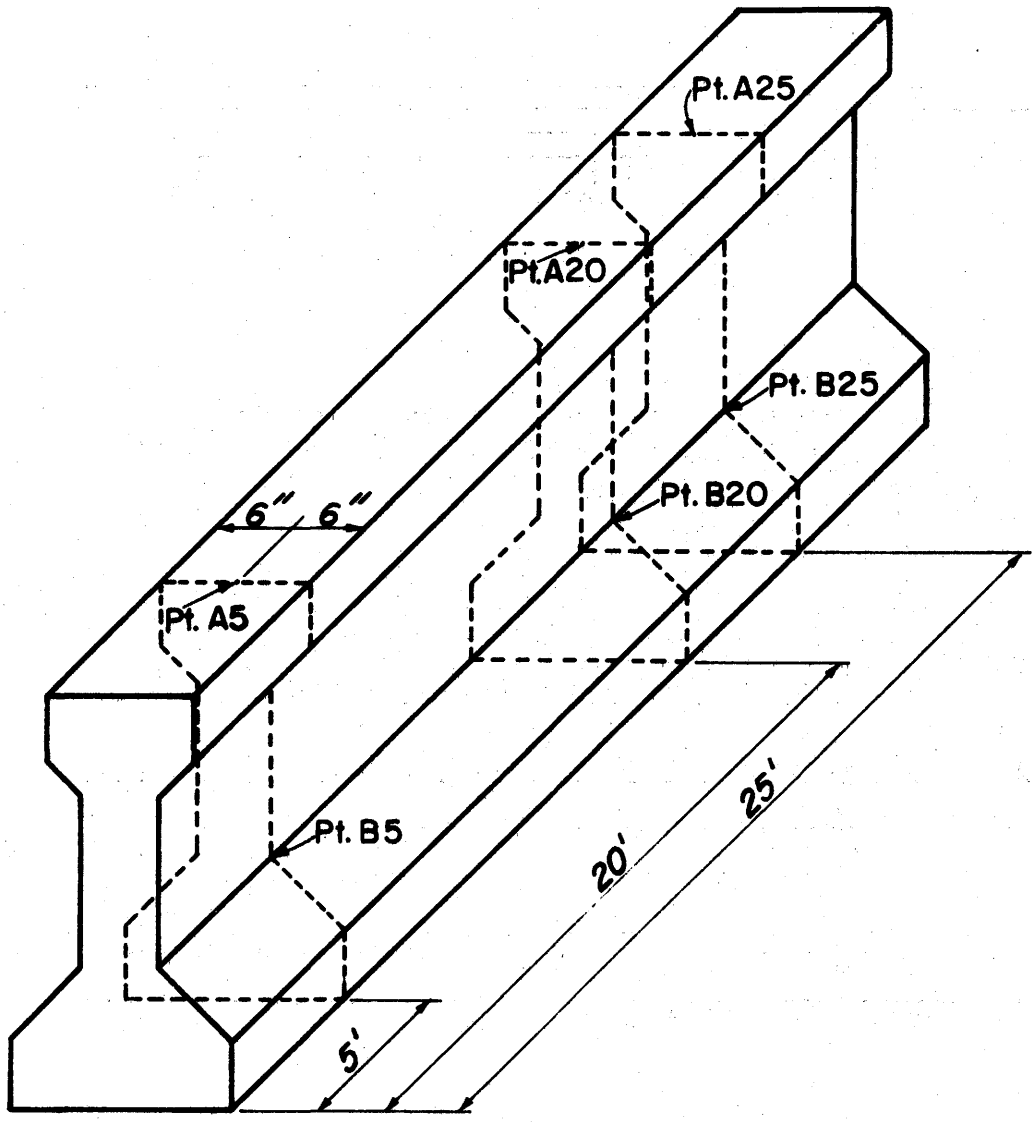

Figure C3.

Normal weight girder at point A20-

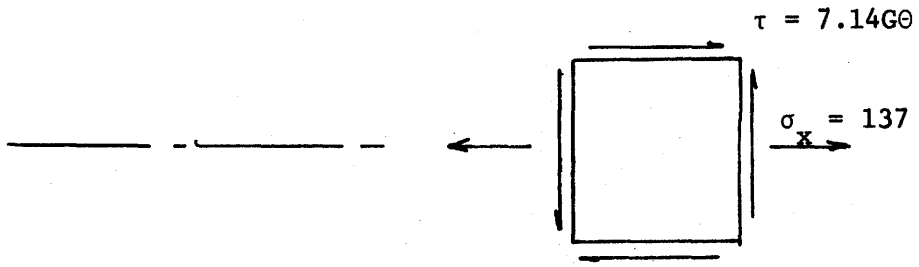

$$\sigma_{1,2} = \frac{\sigma_x}{2} \pm \sqrt{\left(\frac{\sigma_x}{2}\right)^2 + \tau^2}$$

$$\sigma_{1,2} = \frac{137}{2} \pm \sqrt{\left(\frac{137}{2}\right)^2 + (7.14G\Theta)^2}$$

Substitute $G\Theta = \frac{T}{K}$ and adjust for units

$$\sigma_{1,2} = 68.5 \pm \sqrt{4700 + 129T^2}$$

Similiar calculations will result in equations of this form for other points on the surface of the girder.